A neuroprotective agent that inactivates prodegenerative TrkA and preserves mitochondria

Konstantin Feinberg,[1] Adelaida Kolaj,[1,5] Chen Wu,[3] Natalie Grinshtein,[1] Jonathan R. Krieger,[2] Michael F. Moran,[2,4] Lee L. Rubin,[3] Freda D. Miller,[1,4,5] and David R. Kaplan[1,4]

[1]Program in Neurosciences and Mental Health and [2]Program in Cell Biology, Hospital for Sick Children, Toronto, ON, Canada
[3]Department of Stem Cell and Regenerative Biology and Harvard Stem Cell Institute, Harvard University, Cambridge, MA
[4]Department of Molecular Genetics and [5]Department of Physiology, University of Toronto, Toronto, ON, Canada

Axon degeneration is an early event and pathological in neurodegenerative conditions and nerve injuries. To discover agents that suppress neuronal death and axonal degeneration, we performed drug screens on primary rodent neurons and identified the pan-kinase inhibitor foretinib, which potently rescued sympathetic, sensory, and motor *wt* and SOD1 mutant neurons from trophic factor withdrawal-induced degeneration. By using primary sympathetic neurons grown in mass cultures and Campenot chambers, we show that foretinib protected neurons by suppressing both known degenerative pathways and a new pathway involving unliganded TrkA and transcriptional regulation of the proapoptotic BH3 family members BimEL, Harakiri, and Puma, culminating in preservation of mitochondria in the degenerative setting. Foretinib delayed chemotherapy-induced and Wallerian axonal degeneration in culture by preventing axotomy-induced local energy deficit and preserving mitochondria, and peripheral Wallerian degeneration in vivo. These findings identify a new axon degeneration pathway and a potentially clinically useful therapeutic drug.

Introduction

A common occurrence in nerve injuries and neurodegenerative diseases is injury to axons (Neukomm and Freeman, 2014). Axon degeneration is known to be an early feature of many neurological conditions, including Parkinson's disease, amyotrophic lateral sclerosis, Alzheimer's disease, multiple sclerosis, and glaucoma, occurring before the death of the neuronal cell body. The loss of axons is also responsible for the pathology of diabetic and chemotherapy-induced peripheral neuropathy. There are, however, no therapeutic approaches for inhibiting axon loss or for treating the axon degeneration that is responsible for the symptoms and clinical progression of diverse neurological conditions. To develop these approaches, we will need to understand the signaling pathways that mediate axonal loss.

After injury, axons degenerate by two distinct processes. Axons that are proximal to the injury site die back toward the cell body, whereas axons distal to the injury site and no longer connected to the cell body undergo Wallerian degeneration (Adalbert and Coleman, 2013). Both types of degeneration occur after nerve injury and in neurodegenerative conditions, but they are distinct about where on the axon they occur, the timing of degeneration, and, most important, their underlying

molecular mechanisms (Gerdts et al., 2016). In NGF-dependent sympathetic neurons, the receptor-mediated die-back axon degeneration pathway (also known as developmental axon degeneration) is initiated by the loss of NGF-mediated TrkA survival signaling, activation of the p75 neurotrophin receptor, or DR6, which stimulate the dual leucine zipper kinase (DLK)/JNK kinases and the BH3 family members Puma, BimEL, and Harakiri (Hrk), which subsequently compromise mitochondrial function by the activation of Bax, caspase-3 and caspase-6, and calpains (Imaizumi et al., 1997; Putcha et al., 2001; Nikolaev et al., 2009; Park et al., 2010; Simon et al., 2012, 2016). In contrast, Wallerian degeneration involves the Sarm1 adapter protein and kinases of the mitogen-activated protein kinase kinase kinase (MKK)/DLK/JNK pathway, which induce local axonal ATP depletion and activation of calpains (Yang et al., 2015). Although the apoptotic machinery involving the BH3 family members is not important for Wallerian degeneration, JNK is required for a portion of the activities of both pathways (Gerdts et al., 2016).

With the objectives of discovering drugs that inhibit both die-back and Wallerian degeneration and identifying novel axon degeneration signaling pathways, we performed a screen on degenerating primary neurons using a library of drugs known to be safe in humans. One of the drugs we identified, foretinib, a pan-kinase inhibitor (Shi et al., 2009) in clinical trials for

THE JOURNAL OF CELL BIOLOGY

cancer, was very effective in preventing the degeneration of sensory, sympathetic, and motor neurons. Foretinib potently suppressed die-back degeneration, in part by inhibiting a new axon degeneration pathway involving nonliganded and prodegenerative TrkA in axons that ultimately activates the mitochondrial disrupter Bax. Regarding Wallerian degeneration, the effects of foretinib were less robust, with a delay in degeneration in culture and in vivo while suppressing upstream kinases in this pathway. Preservation of mitochondria appears to be key to foretinib's neuroprotective activity.

Results

A kinase inhibitor screen identifies compounds that prevent neuronal death

To identify drugs that prevent axon degeneration, we used NGF deprivation of sympathetic neurons as a model system because loss of axon connectivity to target tissues secreting NGF and other axonal survival factors is thought to occur in neurodegenerative conditions (Adalbert and Coleman, 2013; Gerdts et al., 2016). Specifically, newborn sympathetic neurons from the rat superior cervical ganglion (SCG) were cultured in their obligate survival factor NGF for 6 d in 96-well plates, infected with an EGFP-expressing adenovirus to visualize axons, and then 1 d later were deprived of NGF and treated with a library of kinase inhibitors at 1 µM. The inhibitors consisted of 480 compounds, including 110 in clinical trials or in use in humans (Grinshtein et al., 2011). Axonal degeneration was detectable within 10 h of NGF withdrawal, appearing as swellings along axons, and by 48 h, axonal beading and fragmentation and cell nuclei shrinkage were evident (Fig. 1 A). Neuronal morphology and axon beading/blebbing and fragmentation were assessed at 2, 3, and 4 d after NGF withdrawal (Table 1). Compounds were identified that prevented neuronal death for up to 4 d relative to control neurons withdrawn from NGF, including several against known pro–axon degeneration or antiregeneration proteins, including glycogen synthase kinase 3β, EGFR/erbB, Abl, and JNK (Kaplan and Miller, 2000; Koprivica et al., 2005; Schlatterer et al., 2011) and several targeting Trk (K252a and lestaurtinib) and Met/VEGF receptor (VEGFR; foretinib and sunitinib; Table 1), which have no known roles in mediating axon degeneration.

Foretinib inhibits the degeneration of NGF-dependent sympathetic and sensory neurons

The most effective compound was foretinib, in terms of both the rescue of cell body and axon morphology and the length of time that it protected axons. Foretinib is an orally delivered pan-kinase inhibitor with demonstrated activity in a completed phase II papillary renal cell carcinoma clinical trial (Shah et al., 2013). We therefore compared it with JNK inhibitors, which are known to delay axonal degeneration (Barr et al., 2004). Neonatal mouse sympathetic neurons were cultured in 30 ng/ml NGF for 2 d and withdrawn from NGF using multiple medium changes and the addition of anti-NGF (used in all NGF withdrawal experiments in this study), and 500 nM foretinib was added. Sixteen hours later, neurons were immunostained for βIII-tubulin and counterstained with the nuclear dye Hoechst 33258 to visualize axonal integrity and nuclear morphology. For comparison, neurons were maintained in NGF or were withdrawn from NGF and cultured in the selective JNK inhibitor VII (TAT-TI-JIP$_{153-163}$;

Huntwork-Rodriguez et al., 2013). After NGF withdrawal, axons displayed extensive degeneration, as assessed by the loss of intact neurites (Fig. 1, A and B) and increases in the number of beads on axons (Fig. 1, A and C), and many cell bodies were shrunken and had condensed apoptotic nuclei (Fig. 1, A and D). In contrast, when 500 nM foretinib was added at the time of NGF withdrawal, axons and cell bodies were almost completely rescued from degeneration (Fig. 1, A–D). This rescue was significantly better than that obtained with optimal concentrations of the JNK inhibitor (Fig. 1, A–D; and Fig. S1). A dose response indicated that the most effective concentration of foretinib was 500 nM (unpublished data).

To ascertain the amount of time foretinib could rescue degeneration, NGF-withdrawn rat sympathetic neurons were maintained for 5 or 7 d in foretinib. In the absence of NGF, neurons degenerated completely at both time points, and this degeneration was completely rescued by foretinib at 7 d (Fig. 1 E). We next asked whether foretinib was similarly potent for NGF-dependent developing sensory neurons. Sensory neurons from embryonic day 15 rat dorsal root ganglia (DRGs) were cultured in NGF for 6 d and withdrawn from NGF with or without the addition of foretinib for a further 48 h. Immunostaining for βIII-tubulin demonstrated that in the absence of NGF, sensory axons degenerated significantly over this time period, coincident with cell body shrinkage, and that foretinib rescued these effects (Fig. 1, F–H). Finally, we asked whether foretinib could replace NGF with regard to neuronal survival and axonal maintenance. Rat sympathetic neurons were withdrawn from NGF, cultured for 20 h with or without foretinib, and then switched into NGF alone for a further 2 d. As predicted by previous studies showing that rat sympathetic neurons commit to cell death 16 h after NGF withdrawal (Kristiansen and Ham, 2014), neurons withdrawn from NGF without foretinib degenerated even when NGF was added back after 20 h (Fig. 1 I). In contrast, neurons that were cultured in foretinib over the 20 h of NGF withdrawal were similar in morphology to neurons that had been maintained in NGF over the entire time period (Fig. 1 I). Thus, foretinib can replace NGF with regard to neonatal sympathetic neuron survival and axonal maintenance in culture.

Foretinib promotes the survival of motor neurons

To determine whether foretinib protected neurons that were not NGF dependent, we examined mouse motor neurons. Motor neurons were generated from an embryonic stem (ES) cell line derived from mice carrying a transgenic reporter gene in which GFP is driven by promoter elements from the motor neuron-specific *Hb9* gene (*Hb9*::GFP; Di Giorgio et al., 2007). Motor neurons were generated using established protocols (Yang et al., 2013b), culturing the newly generated dissociated motor neurons in basal conditions including the trophic factors glial cell-derived neurotrophic factor, brain-derived neurotrophic factor, and ciliary neurotrophic factor (20 µg/ml) for 3 d and then for an additional 9 d with or without trophic factors and with or without foretinib. Motor neurons were then quantified by counting GFP-positive cells. The trophic factors supported the survival of many *Hb9*::GFP-positive motor neurons over this time period, and in their absence, virtually all motor neurons died (Fig. 2 A). Foretinib rescued this cell death in a concentration-dependent fashion, with maximal survival at 500 nM (Fig. 2 B).
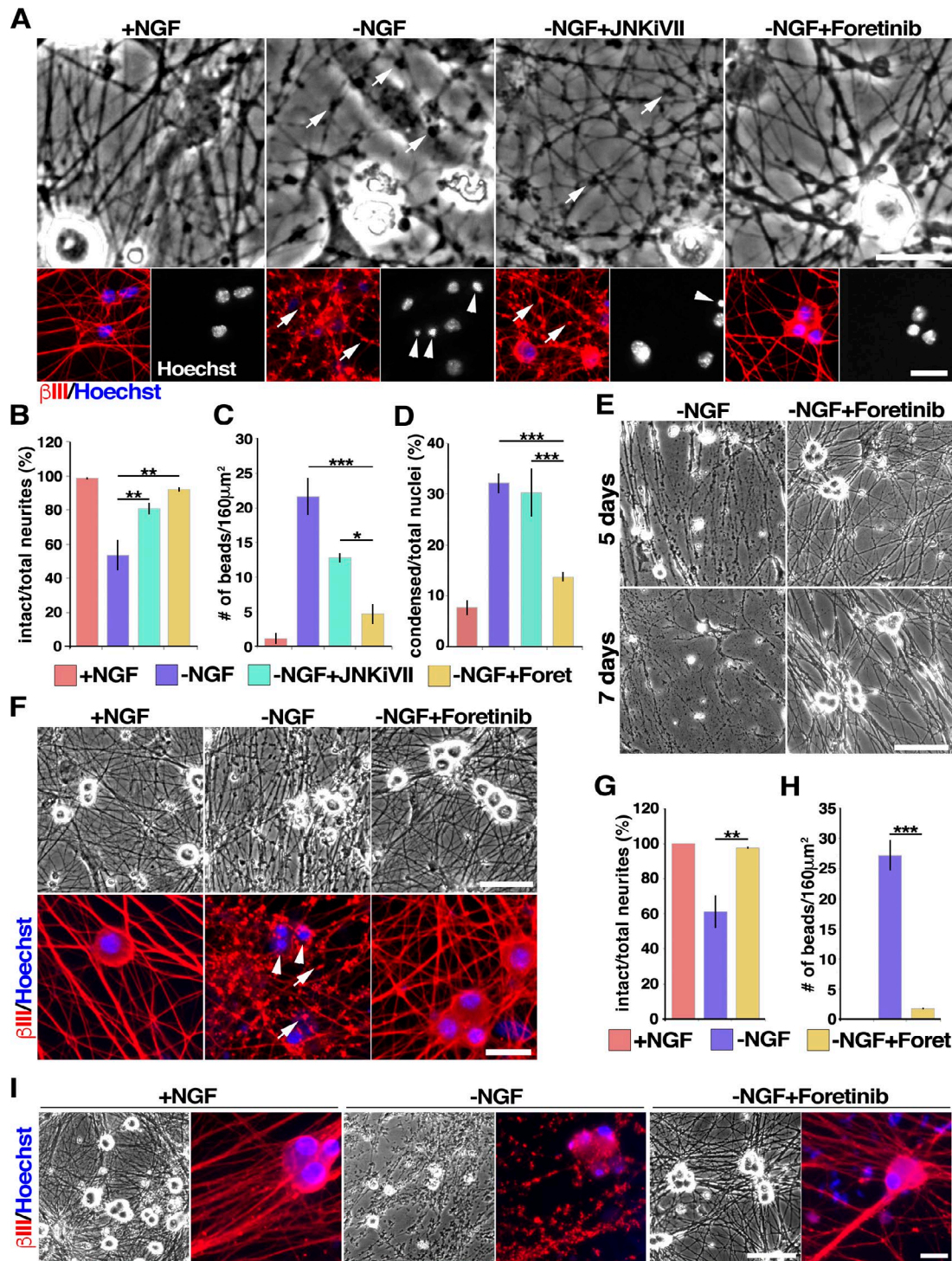
Figure 1. **Foretinib prevents NGF-induced death and degeneration of sympathetic and sensory neurons.** (A–D) Foretinib protects sympathetic neurons from degeneration more effectively than a JNK inhibitor. Murine sympathetic neurons were cultured in NGF for 2 d, withdrawn from NGF (−NGF), and cultured for 16 h with or without 2 µM JNK inhibitor TAT-TI-JIP$_{153-156}$ (JNKiVII), 500 nM foretinib (Foret), or NGF. Shown is immunostaining for βIII-tubulin (red) and costaining with Hoechst 33258 to highlight nuclear morphology (bottom) or bright-field (top) panels. Images were quantified as described in Materials and methods for the number of intact neurites (B), axonal beads (C), or condensed apoptotic nuclei (D). *, P < 0.05; **, P < 0.01; ***, P < 0.005. Arrows in A denote axonal beading, indicative of degenerating axons, and arrowheads shrunken, apoptotic nuclei. (E) Foretinib protects sympathetic neurons from NGF withdrawal–induced degeneration for up to 7 d. (F–H) Foretinib protects sensory neurons. Mouse sensory neurons withdrawn from NGF were cultured for a further 48 h with or without 500 nM foretinib. Arrows denote axonal beading and arrowheads shrunken, apoptotic nuclei. (G and H) Images as in F were quantified for degeneration as described for B and C, respectively. **, P < 0.01; ***, P < 0.005; n = 3 independent experiments. (I) Rat sympathetic neurons cultured in foretinib over the 20 h of NGF withdrawal are similar in morphology to neurons maintained in NGF. Bars: (A, both panels; and F, bottom) 25 µm; (F, top) 60 µm; (E and I, bright-field images) 100 µm; (I, immunofluorescence images) 20 µm. Error bars represent mean ± SEM.

To better characterize this survival effect, a time-course analysis of motor neuron survival with 500 nM foretinib was performed (Fig. 2 C). When trophic factors were withdrawn 3 d after dissociation, all motor neurons died by 8 d (11 d after dissociation). Although the trophic factors partially rescued motor neuron survival over this time course, the most robust survival was observed with foretinib, with half of the neurons remaining in foretinib compared with none in the trophic factor–withdrawn cultures at 11 d after dissociation (Fig. 2 C). Quantification showed that 3 d after trophic factor withdrawal (6 d after dissociation), foretinib was significantly better than the optimized trophic factors at rescuing motor neuron survival (Fig. 2 D).

These data indicate that foretinib is a potent motor neuron survival agent, and we therefore asked whether it could also rescue the survival of compromised motor neurons. ES cell–derived motor neurons were generated that carried both the *Hb9*::GFP reporter gene and a transgene encoding a human *SOD1* gene with a G93A mutation that is found in amyotrophic lateral sclerosis (*SOD1*[G93A]; Makhortova et al., 2011; Yang et al., 2013b). As seen with the *Hb9*::GFP motor neurons, 9 d after dissociation, foretinib promoted the survival of *SOD1*[G93A]; *Hb9*::GFP motor neurons in a dose-dependent fashion, with motor neuron survival increased almost 20-fold at 500 nM (Fig. 2, E and F). A time-course analysis demonstrated that at 3 d after trophic factor withdrawal (6 d after dissociation), almost all of the *SOD1*[G93A]; *Hb9*::GFP motor neurons had died, and 500 nM foretinib rescued this cell death by almost fourfold (Fig. 2, G and H). At 6 d of trophic factor withdrawal (9 d after dissociation), all neurons had died, whereas 10% were viable in trophic factor and 40% in foretinib. At 15 d after dissociation (the longest time point analyzed), <10% of neurons were viable in trophic factor, 35% were viable in foretinib, and >50% were viable in the presence of both foretinib and trophic factors (Fig. 2 G).

Foretinib locally prevents axonal degeneration after NGF withdrawal in culture

We next asked whether foretinib acts locally on axons to prevent degeneration. To distinguish neuronal survival from axonal maintenance, we used compartmented cultures of sympathetic neurons, which allow independent manipulation of cell bodies and distal axons (Campenot, 2009). To determine whether foretinib could locally protect axonal integrity, we established

neonatal rat sympathetic neurons for 6 d with 20 ng/ml NGF in all compartments, withdrew NGF from both axonal side compartments, and then added foretinib to one side compartment and vehicle alone to the other. Neuronal cell bodies remained alive because of the NGF in the central compartment. Immunostaining for βIII-tubulin showed that distal axons in the side compartment deprived of NGF displayed swelling by 10 h and massive axonal beading and breakage at 48 h (Fig. 3 Ai). In contrast, the distal axons in the other side of the same compartments that were deprived of NGF but with foretinib were intact at both time points (Fig. 3 Ai). Thus, foretinib locally inhibits axonal degeneration due to NGF withdrawal.

We next asked whether foretinib could maintain axonal integrity even when neuronal cell bodies were dying. To do this, we withdrew NGF from all compartments, followed by incubation with anti-NGF, and added foretinib to one side compartment. Analysis 2 d later by immunostaining for βIII-tubulin demonstrated that in the absence of NGF, axons degenerated, as quantified by counting axonal swellings (Fig. 3, Aii and B). In contrast, in the side compartments containing only foretinib, axonal integrity was completely maintained, despite cell bodies' being shrunken and apoptotic in the absence of NGF in the cell body compartment (Fig. 3, Aii and B). Foretinib can therefore maintain axonal integrity acting locally even when cell bodies are dying. We next asked whether foretinib, added only to axons in one of the side compartments and the cell body compartment, could rescue the NGF withdrawal–induced degeneration of axons in the other side compartment. Foretinib in the cell body compartment efficiently rescued axons in the distal compartment (Fig. 3 Aiii). These findings indicate that foretinib can signal anterogradely from the cell body to axons to suppress degeneration mediated by NGF withdrawal, perhaps by inhibiting a cell body–driven anterograde-axonal death process.

Foretinib suppresses signaling pathways associated with mitochondrial-dependent neuronal death and axon degeneration

To gain molecular insights into foretinib's antidegenerative activity, we performed transcriptome analysis on sympathetic neurons that were withdrawn from NGF with or without concomitant foretinib treatment. Specifically, we cultured neonatal rat sympathetic neurons in NGF for 6 d and then withdrew them from NGF for 8 h with or without foretinib. For comparison, sister

Table 1. **Rescue of NGF deprivation–induced neuronal death and degeneration by tyrosine kinase inhibitors**

Target kinase	Inhibitor	Subjective survival rate		
		Day2	Day3	Day4
GSK3β	CT99021	++	++	+/−
	CHIR98014 isomer	++	+	+/−
	TWS119	++	+	−
BCR, Abl, Src	Ponatinib	+++	++	+
TrkA	K-252a	++	+	+
	Lestaurtinib	+++	++	++
JNK	SP-600125	++	++	+
EGFR, HER2	CI-1033	++	++	+
	Tyrphostin B44	+++	++	++
MET, VEGFR	Sunitinib malate	+++	++	++
	Foretinib	++++	++++	++++

Neonatal rat sympathetic neurons withdrawn from NGF for 6 h were cultured without NGF and with 1 μM of tyrosine kinase inhibitors for 2–4 d more. Survival and axonal integrity was subjectively estimated on each day. "++++" cultures with morphology comparable with those maintained in NGF; "−" cultures similar to NGF-withdrawn untreated cultures.
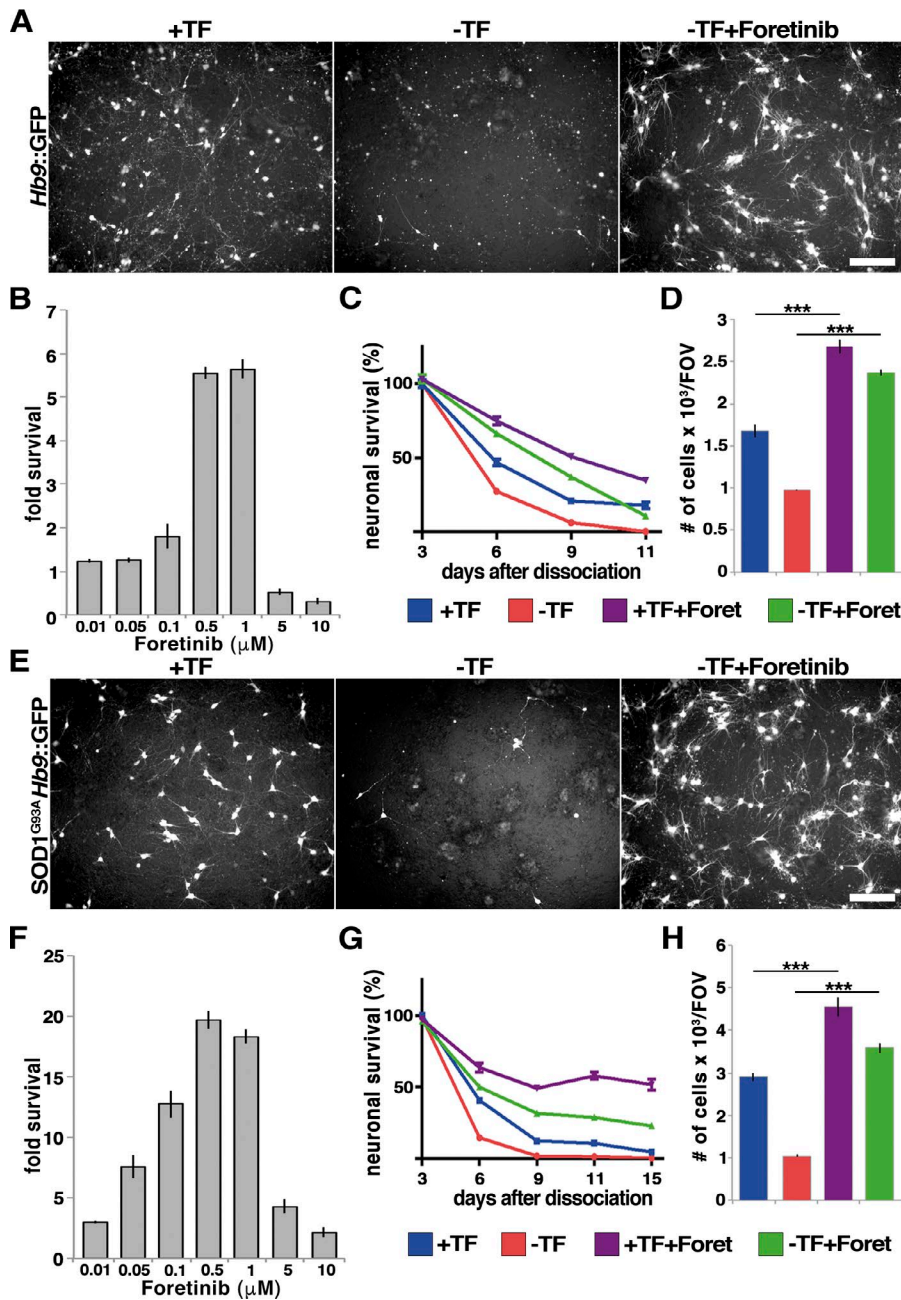
Figure 2. **Foretinib promotes survival of wild type and mutant SOD1 motor neurons.** (A–D) Motor neurons (Hb9::GFP) generated as described in Materials and methods were switched into medium with or without trophic factors (TFs) or foretinib (Foret). (A) Live images of motor neurons cultured for 9 d with or without TF or 500 nM Foretinib. (B) Proportion of surviving motor neurons expressed as the fold increase relative to those from cultures grown without TFs or foretinib; $n \geq 3$ independent experiments. (C) Percentage of surviving motor neurons over time with or without TFs or 500 nM foretinib; $n \geq 3$ independent experiments. (D) Number of surviving GFP-positive motor neurons in cultures 3 d after TF withdrawal and 500 nM foretinib addition. ***, $P < 0.005$; $n \geq 3$ independent experiments. (E–H) Motor neurons generated from $SOD1^{G93A}/Hb9$::GFP murine ES cells were switched into medium with or without TFs in the presence or absence of 500 nM foretinib. (E) Live images of $SOD1^{G93A}/Hb9$::GFP mouse motor neurons cultured in the indicated conditions for 9 d. (F) Proportion of surviving $SOD1^{G93A}$ motor neurons expressed as the fold increase relative to those from cultures grown without TFs or foretinib; $n \geq 3$ independent experiments. (G) Percentage of surviving motor neurons over time; $n \geq 3$ independent experiments. (H) Number of surviving GFP-positive motor neurons 3 d after TF withdrawal and 500 nM foretinib addition. ***, $P < 0.005$; $n \geq 3$ independent experiments. Bars, 100 µm. Error bars represent mean ± SEM.

cultures were maintained in NGF. RNA was extracted from these samples and analyzed on Rat Gene 2.0 ST arrays. A differential gene expression analysis identified 1,056 mRNA transcripts with >1.2-fold change in NGF withdrawn neurons with and without foretinib (Fig. S2 A and Table S2). Unbiased hierarchical clustering (using the complete-linkage method) of a Euclidean distance matrix of $\log_2$-normalized expression data (Naska et al., 2016) demonstrated that the replicates within each population clustered closely (Fig. S2 A), validating the comparison. Moreover, this analysis demonstrated that gene expression of NGF-withdrawn neurons treated with foretinib clustered more closely with neurons maintained in NGF than with untreated NGF-withdrawn neurons (Fig. S2 A), suggesting that foretinib globally inhibited transcriptional changes associated with NGF withdrawal.

Among the top differentially expressed genes in this comparison were those encoding the proapoptotic BH3 family members BimEL, Hrk, Pmaip1/Noxa, and the growth arrest and DNA damage–inducible, apoptosis-associated Gadd45γ. The mRNAs for these genes have been previously reported to be elevated after NGF withdrawal of sympathetic neurons (Imaizumi et al., 1997; Kojima et al., 1999; Putcha et al., 2001; Kristiansen and Ham, 2014), and BimEL and Hrk are rate limiting for sympathetic neuron apoptosis (Putcha et al., 2001; Whitfield et al., 2001; Towers et al., 2009). To confirm that the expression of these mRNAs was indeed suppressed by foretinib treatment, we performed quantitative RT-PCR at 9–12 h after NGF withdrawal, when they are known to be maximally elevated in sympathetic neurons. We also examined the mRNA encoding TAp63, a p53 family member that we previously showed was required for the apoptosis of sympathetic neurons deprived of NGF (Jacobs et al., 2005), as well as those encoding Puma, ddit3, and trib3, all of which have been associated with neuronal apoptosis and/or
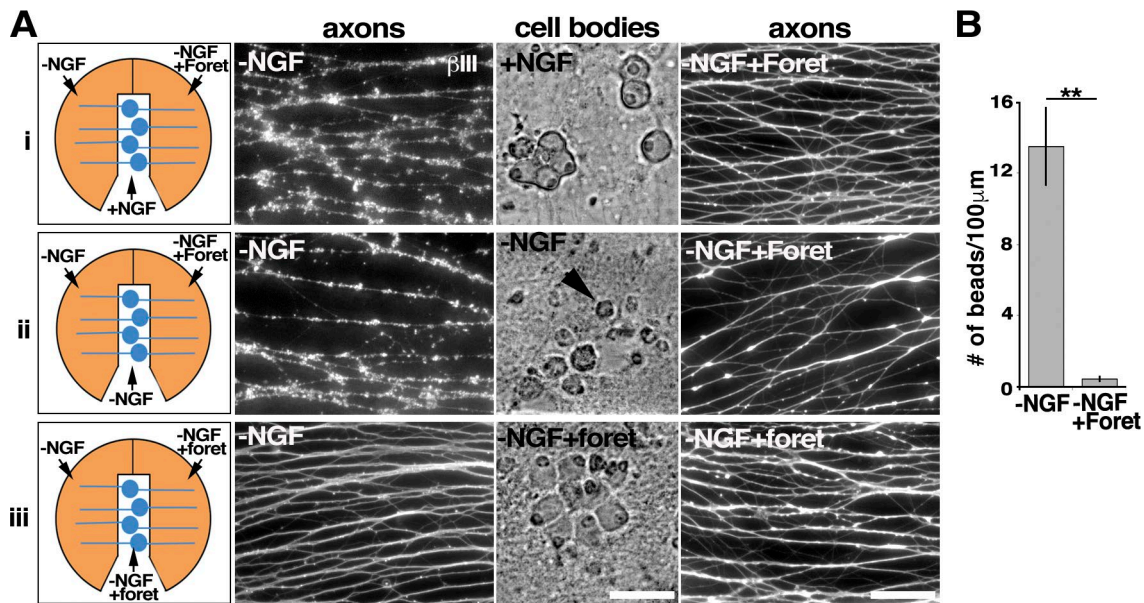
Figure 3. **Foretinib inhibits local sympathetic axon degeneration caused by trophic factor deprivation.** (A) Rat sympathetic neurons were switched into the indicated conditions for 48 h and immunostained for βIII-tubulin (white). Schematics on the left show the configurations used. In the top panels (i), NGF was maintained in the center compartment and removed from both side compartments, and 500 nM foretinib (Foret) added to one of the sides. In the center and bottom panels (ii and iii), NGF was withdrawn from all compartments, and foretinib added to one of the sides (ii) or one of the sides and the center compartment (iii). Fluorescence images show βIII-tubulin–positive axons in the two sides of the same compartments, and the bright-field images the cell bodies and proximal axons in the center compartments of the same cultures. Arrowhead denotes a shrunken, dying neuron. (B) Number of swellings or beads per 100 µm of neurite in the side compartments withdrawn from NGF with and without 500 nM foretinib. **, P < 0.01; n ≥ 3 independent experiments. Bars, 50 µm. Error bars represent mean ± SEM.

axon degeneration (Besirli et al., 2005; Galehdar et al., 2010; Kristiansen et al., 2011; Ghosh et al., 2012; Zareen et al., 2013; Simon et al., 2016). This analysis confirmed that these mRNAs were increased after NGF withdrawal and showed that, in every case, foretinib suppressed their NGF withdrawal–induced up-regulation (Fig. 4, A and B).

Puma expression in the cell soma is retrogradely up-regulated in response to trophic factor deprivation in axons and subsequently acts anterogradely to induce the degeneration of these axons (Simon et al., 2016). We therefore asked whether foretinib, added only to NGF-deprived axons, prevents retrograde prodegenerative signaling that induces expression of *puma* in the cell body. In compartmental cultures, NGF was withdrawn from all compartments, and foretinib was added only to both axonal compartments for 24 h (Fig. S2 B). Quantitative RT-PCR analysis performed on mRNA isolated from the cell bodies revealed that foretinib added to axons inhibited the expression of *puma* in the cell body, compared with the control untreated cultures (Fig. S2 C).

Proapoptotic BH3 family members are known components of a pathway that is essential for NGF withdrawal–induced sympathetic neuron apoptosis and axon degeneration that involves the upstream kinase JNK (Whitfield et al., 2001; Towers et al., 2009; Kristiansen and Ham, 2014). We therefore asked if foretinib suppressed this pathway. We first examined JNK activity, analyzing mouse sympathetic neurons that were withdrawn from NGF for 10–12 h with or without foretinib. As demonstrated by Western blot (WB) analysis with an antibody to phosphorylated and activated JNK (Fig. 4 C and Table S1), phosphorylated JNK was increased by NGF withdrawal, as was the direct JNK target, phosphorylated c-jun (Fig. S2 D and Table S1), and these increases were completely suppressed by foretinib. Second, we asked about two proapoptotic BH3 family

members implicated in sympathetic neuron apoptosis: BimEL, a target of JNK that acts to inhibit the prosurvival family members Bcl-2, Bcl-xL, and Bcl-w (Putcha et al., 2001, 2003), and Bax, which permeabilizes mitochondria during apoptosis and axon degeneration and is also activated by BimEL, Noxa and Puma (Putcha et al., 1999). WB analysis (Fig. 4 D, Fig. S2 E, and Table S1) showed that at four different time points after NGF withdrawal, BimEL protein levels were increased and that this increase was completely suppressed by foretinib, consistent with the quantitative RT-PCR analysis. Similarly, analysis using nondenaturing conditions showed that the levels of the conformationally active form of Bax (Upton et al., 2007) were increased by NGF withdrawal and that this was partially suppressed by foretinib (Fig. 4 E and Table S1).

Because BimEL and Bax activity result in compromised mitochondria, we next assayed mitochondrial outer membrane permeabilization by measuring the release of cytochrome *c* by immunostaining (Deshmukh and Johnson, 1998; Neame et al., 1998; Jacobs et al., 2005). We quantified the number of βIII-tubulin positive neurons displaying lost or diffuse/uniform cytochrome *c* staining, which is indicative of its extrusion from the mitochondria upon NGF deprivation, and found that this was prevented by foretinib treatment (Fig. 4, H and I). This observation was supported by WB analysis showing that cytosolic (vs. mitochondrial) cytochrome *c* levels were increased after NGF withdrawal and that this increase was partially suppressed by foretinib (Fig. S2 F). Because cytochrome *c* release initiates a caspase cascade that regulates sympathetic neuron apoptosis and axon degeneration (Deshmukh and Johnson, 1998; Slee et al., 1999), we also examined cleavage and activation of caspase-3, required for axon degeneration (Simon et al., 2012). WBs of sympathetic neuron lysates 10–12 h after NGF withdrawal (Fig. 4 F, Fig. 5 H, and Table S1) together with
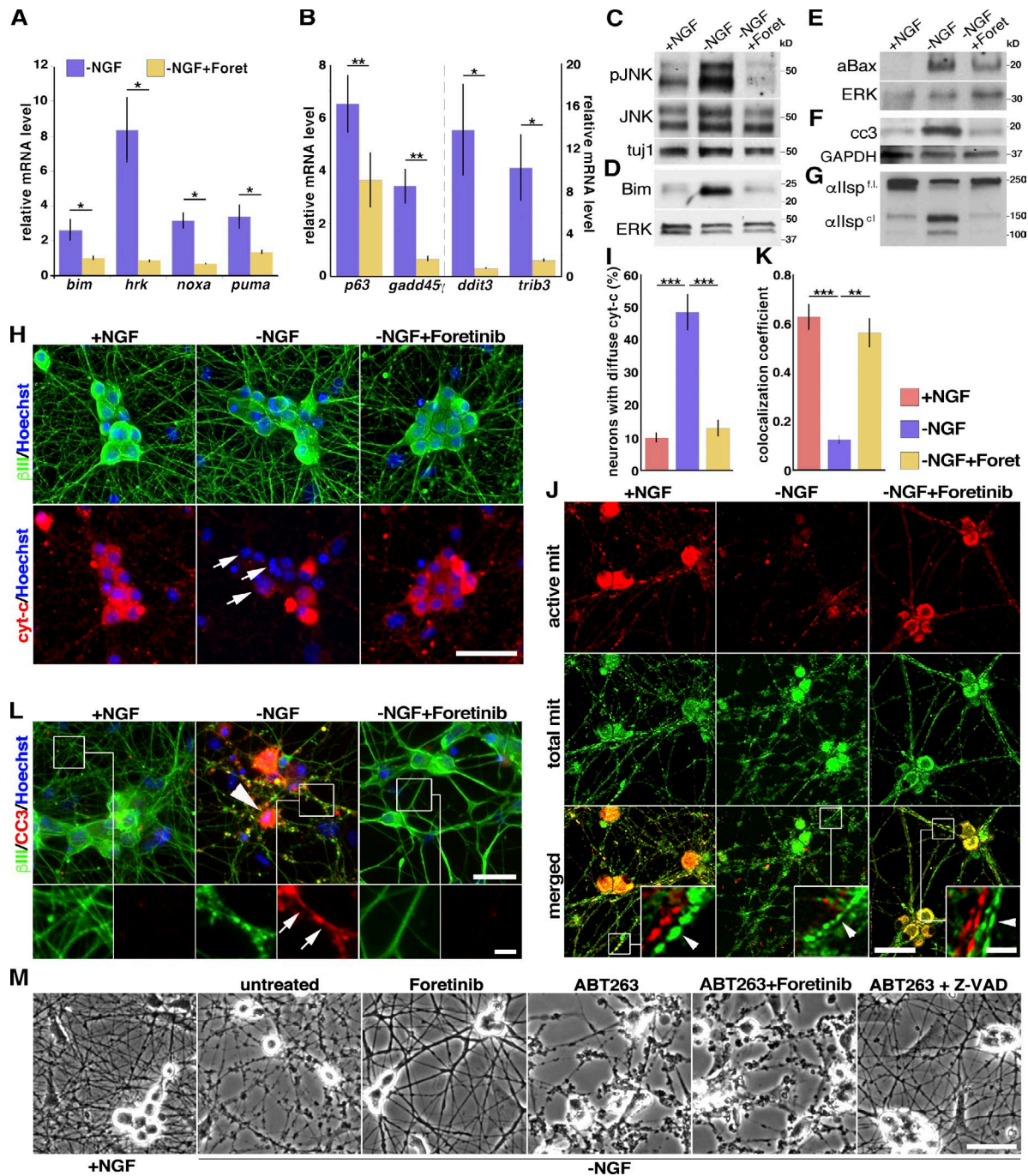
Figure 4.   **Foretinib suppresses the expression or activity of genes and proteins associated with sympathetic neuron death and degeneration and protects mitochondria.** (A and B) Changes in gene expression in mouse sympathetic neurons withdrawn from NGF for 9 h (*bimEL, puma/bbc3, trib3, ddit3,* and *hrk* mRNAs) or 12 h (*pmaip1/noxa, gadd45γ, tap63* mRNAs) with or without foretinib (Foret) by quantitative RT-PCR; $n \geq 3$ independent experiments. (C–G). WB analysis of mouse sympathetic neurons withdrawn from NGF with or without 500 nM foretinib for 10–12 (C and F), 18 (D and E), or 24 (G) h. Blots were probed with antibodies to the indicated proteins, including phosphorylated (p) JNK, activated (a) Bax, cleaved caspase-3 (cc3), or αII-spectrin (cleaved [cl] and full-length [f.l.]), and reprobed for βIII-tubulin (tuj1), ERK1/2, or GAPDH to control for loading. (H and I) Mouse sympathetic neurons withdrawn from NGF in the presence or absence of foretinib for 12 h, immunostained for cytochrome *c* (red, cyt-c) or βIII-tubulin (green), and quantified for neurons with diffuse cytochrome *c* (I), as indicated by arrows in H. (I) ***, P < 0.001; $n = 3$. (J and K) Foretinib protects mitochondria. Mouse sympathetic neurons withdrawn from NGF in the presence or absence of foretinib for 24 h were stained as live cells with MitoTracker Green FM (green) and MitoTracker Red CMXRos (red), which label total and active mitochondria (mit), respectively. Boxed regions are shown in higher magnification in the insets, with the red and green channels split to show the double-labeling of mitochondria in axons (arrowheads). (K) Signal colocalization of active and total mitochondria, as in J. **, P < 0.01; ***, P < 0.001; $n = 3$. (L) Mouse sympathetic neurons withdrawn from NGF in the presence or absence of foretinib for 24 h and immunostained for cleaved caspase-3 (red, CC3) and βIII-tubulin (green). Boxed regions are shown at higher magnification in the bottom row to show cleaved caspase-3 in axons (arrows). Arrowhead indicates apoptotic cell body. (M) Neuroprotection by foretinib requires the Bcl2 family. Bright-field micrographs for mouse sympathetic neurons withdrawn from NGF for 16 h and 500 nM foretinib, 10 µM ABT-263 (Bcl2 family inhibitor), and/or 100 µM Z-VAD (caspase inhibitor) added. Bars: (H, M, and J, main images) 50 µm; (J, zoomed-in insets) 10 µm; (L, top) 25 µm; (L, bottom) 5 µm. Error bars represent mean ± SEM.
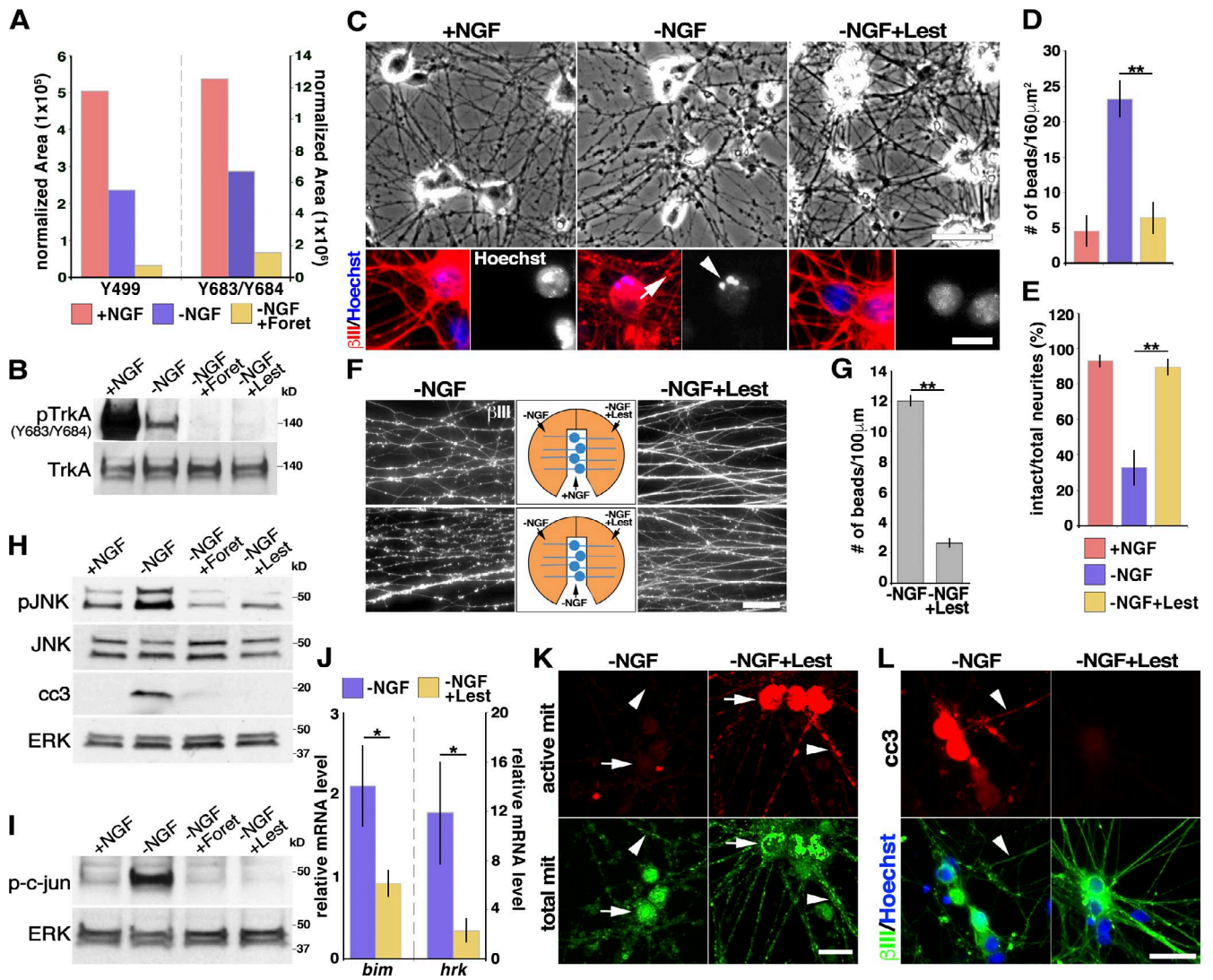
Figure 5. **Foretinib and lestaurtinib inhibit the low levels of TrkA tyrosine phosphorylation in NGF-deprived neurons and suppress axon degeneration.** (A) Quantitative normalized representation of the phosphoproteomics analysis performed on rat sensory neurons in the indicated conditions for 8 h, showing the relative amount of TrkA peptides containing phosphorylated Y499 (Shc binding site) or Y683 and Y684 (activation loop tyrosines). (B) WB analysis of mouse sympathetic neurons withdrawn from NGF with or without 500 nM foretinib (Foret) or 1 µM Lestaurtinib (Lest) for 10 h, probed for TrkA phosphorylated at Y683/Y684, and reprobed for total TrkA. (C) Mouse sympathetic neurons withdrawn from NGF in the presence or absence of 1 µM lestaurtinib for 24 h and immunostained for βIII-tubulin (red) and counterstained with Hoechst 33258 (blue; bottom) and bright-field (top). The arrow indicates neuritic beading and the arrowhead an apoptotic cell. (D and E) Images as in C quantified for the number of swellings or beads (D) and the ratio of intact neurites (E). **, P < 0.01; n ≥ 3 independent experiments. (F) The Trk inhibitor lestaurtinib locally protects rat sympathetic neuron axons in compartmented cultures. (Top) NGF was maintained in the center compartment and removed from both side compartments, and 1 µM lestaurtinib added to one of the two sides for 48 h. (Bottom) NGF was withdrawn from all compartments, and lestaurtinib was added to one of the two sides. The fluorescence images show βIII-tubulin–positive axons in the two sides of the same compartments. (G) Quantification of axon degeneration of the bottom panels of F. **, P < 0.01; n ≥ 3 independent experiments. (H and I) WB analysis of mouse sympathetic neurons withdrawn from NGF with or without 500 nM foretinib or 1 µM lestaurtinib for 10 h, probed for phosphorylated or total JNK and cleaved caspase-3 or phosphorylated c-jun, and reprobed for total ERK1/2 as a loading control. (J) Changes in levels of *bimEL* and *hrk* mRNAs in mouse sympathetic neurons withdrawn from NGF for 9 h and analyzed by quantitative RT-PCR; n = 5 independent experiments. (K) Representative images of mouse sympathetic neurons withdrawn from NGF in the presence or absence of lestaurtinib for 24 h, and stained as live cells with MitoTracker Green FM (green) and MitoTracker Red CMXRos (red), which label total and active mitochondria (mit), respectively. Arrows indicate cell bodies and arrowheads axons. (L) Images of mouse sympathetic neurons withdrawn from NGF with or without lestaurtinib for 24 h, and immunostained for βIII-tubulin (green) and cleaved caspase-3 (red, cc3). Arrowheads indicate neurites with cleaved caspase-3 immunoreactivity. Bars: (F, K, and C, top) 50 µm; (C, bottom) 15 µm; (L) 25 µm. Error bars represent mean ± SEM. All WB experiments were performed a minimum of three times, with representative blots shown.

immunostaining of sympathetic neuron cultures withdrawn from NGF for 24 h (Fig. 4 L and Fig. S3 B) showed that cleaved caspase-3 levels were robustly increased and that this increase was completely suppressed by foretinib. Finally, we asked about the cleavage of αII-spectrin, which is downstream of calpain and caspase activation during NGF withdrawal–induced

death (Yang et al., 2013a, 2015). At 24 h after NGF withdrawal, αII-spectrin cleavage was almost eliminated by foretinib treatment (Fig. 4 G and Table S1).

These data suggest that foretinib potently suppresses NGF withdrawal–induced neuronal death and degeneration by inhibiting the molecular pathway underlying the integrity of

mitochondria. To directly demonstrate the involvement of neuronal mitochondria, and to ask whether this protection occurs in cell bodies and/or axons, we assessed mitochondrial status in cultured sympathetic neurons in the presence or absence of foretinib. Mouse sympathetic neurons were withdrawn from NGF for 24 h and incubated with MitoTracker Green FM and MitoTracker Red CMXRos, which label total and active mitochondria, respectively, with the latter only accumulating in mitochondria in response to the highly negative mitochondrial membrane potential. In neurons withdrawn from NGF, very few active mitochondria were observed (Fig. 4 J, middle; and Fig. S3 A). In contrast, there were abundant active mitochondria in cell bodies and axons of neurons maintained in NGF or withdrawn from NGF for 24 h in the presence of foretinib (Fig. 4, J [left and right] and K; and Fig. S3 A).

These findings suggest that foretinib acts on axons and cell bodies to inhibit proapoptotic BH3 family member expression and activity and in so doing protect mitochondria. To further test this hypothesis, we predicted that foretinib would not protect neurons from degeneration when the activity of the antiapoptotic Bcl-2 family members Bcl-2, Bcl-xL, and Bcl-w were inhibited. Sympathetic neurons were withdrawn from NGF for 16 h and treated with the selective Bcl-2/Bcl-xL/Bcl-w inhibitor ABT-263 (Tse et al., 2008) in the presence or absence of foretinib. For comparison, we used the caspase inhibitor Z-VAD-FMK, which should rescue NGF-deprived sympathetic neurons in the presence of ABT-263, because caspase activation occurs downstream of BH3 family member activity (Chang et al., 2002). Foretinib rescued NGF withdrawal–induced degeneration in the absence but not presence of ABT-263 (Fig. 4 M). In contrast, Z-VAD-FMK rescued the neurons even in the presence of ABT-263. Thus, foretinib inhibits proapoptotic BH3 family members, which then enables antiapoptotic BH3 family members to preserve mitochondria.

Foretinib functions in part by inhibiting unliganded TrkA-mediated degenerative activity in NGF-deprived neurons

To identify targets of the pan-kinase inhibitor foretinib in neurons, we performed a phosphoproteomics analysis of E15 rat sensory (DRG) neurons cultured for 6 d in NGF. Neurons were withdrawn from NGF and incubated with anti-NGF, and 500 nM foretinib was added for 8 h. Before lysis, neurons were treated for 10 min with sodium orthovanadate to preserve phosphotyrosine. Lysates were subjected to tryptic digestion, phosphopeptides enriched with phosphotyrosine antibody, and eluted peptides analyzed by MS/MS. Foretinib quantitatively inhibited the tyrosine phosphorylation of TrkA (Fig. 5 A) and PLCγ1, a direct target of TrkA-mediated tyrosine phosphorylation (Kaplan and Miller, 2000; Fig. S4 A). The phosphopeptides in TrkA inhibited by foretinib included those containing the Shc binding site (pY499) and activation loop transphosphorylation sites (pY683 and pY684; Fig. 5 A and Fig. S4 A). Although foretinib is best known as a Met and VEGFR2 inhibitor, it has been reported to inhibit TrkA with a similar potency (Shi et al., 2009). Of the known foretinib targets, only the tyrosine phosphorylation of TrkA was found to be inhibited by foretinib in NGF-deprived sensory neurons in our phosphoproteomics analysis (unpublished data).

To confirm these findings, we analyzed lysates of mouse sympathetic neurons deprived of NGF in the presence or absence of foretinib by immunoblotting with an antibody to the Y683/Y684 transphosphorylation sites of TrkA responsible for receptor activation (Kaplan and Miller, 2000). A small but consistent level of TrkA tyrosine phosphorylation was observed in neurons withdrawn from NGF and incubated in anti-NGF, and this was completely suppressed by foretinib (Fig. 5 B and Table S1). Similar results were observed by immunoblotting with an antibody to the Y785 phosphorylation site of TrkA responsible for tyrosine phosphorylation and activation of PLCγ1 (Kaplan and Miller, 2000). Again, there was a small but consistent level of TrkA Y785 phosphorylation in neurons withdrawn from NGF that was suppressed by foretinib (Fig. S4 B). This finding is consistent with reports that TrkA can transphosphorylate in the absence of ligand, albeit inefficiently (Kaplan et al., 1991; Cunningham et al., 1997), and raises the question of whether kinase-active TrkA can, under some circumstances, induce the death of cell bodies or axons, as it does in pediatric neural tumor cells even in the absence of ligand (Harel et al., 2009).

To begin to address this possibility, we focused upon lestaurtinib (CEP-701), a pan-Trk inhibitor (Miknyoczki et al., 1999), because it was identified in our kinase library screen as having antidegeneration activity (Table 1). Sympathetic neuron cultures were withdrawn from NGF in the presence or absence of 1 µM lestaurtinib. Analysis 24 h later showed that lestaurtinib suppressed the neuronal apoptosis and axon degeneration that occurred after NGF withdrawal at this time point (Fig. 5, C–E). To differentiate lestaurtinib's effects on sympathetic neuron cell bodies versus axons, we established compartmented cultures, withdrew NGF from both side compartments, and added lestaurtinib to just one side compartment. In one set of experiments, we maintained NGF in the center compartment, whereas in a second, we withdrew it. βIII-Tubulin immunostaining at 48 h showed that when NGF was present in the center compartment, there was less axon degeneration in the NGF-withdrawn side that contained lestaurtinib than in the side compartment without this drug (Fig. 5 F, top). Moreover, even when NGF was withdrawn from all compartments, 2 d of lestaurtinib treatment significantly rescued distal axons when added to the distal axon compartment (Fig. 5, F [bottom] and G). It is unlikely that lestaurtinib mediates these effects by inhibiting its other targets Flt3 or JAK2, because we did not find either of these proteins phosphorylated in NGF-deprived sympathetic neurons in our phosphoproteomics analysis (unpublished data). Lestaurtinib also has no reported inhibitory effect on MKK/JNK family kinases.

Several lines of evidence suggested that lestaurtinib might act like foretinib in suppressing sympathetic neuron degeneration. First, quantitative RT-PCR analysis of mouse sympathetic neurons withdrawn from NGF for 9 h with and without lestaurtinib showed that the drug inhibited the NGF withdrawal–induced increase in *bimEL* and *hrk* mRNAs (Fig. 5 J). Second, WB analysis demonstrated that like foretinib, lestaurtinib suppressed the phosphorylation and activation of JNK seen 10 h after NGF withdrawal, as well as the phosphorylation of its direct target c-jun (Fig. 5, H and I; and Table S1). Third, when sympathetic neurons were withdrawn from NGF for 24 h and stained with MitoTracker Green FM and MitoTracker Red CMXRos, coincident lestaurtinib treatment rescued the loss of active mitochondria seen after NGF withdrawal (Fig. 5 K and Fig. S3 A). Finally, immunostaining showed that like foretinib, lestaurtinib suppressed the NGF withdrawal–induced appearance of cleaved caspase-3 in the axons and cell bodies of sympathetic neurons (Fig. 5, H and L; Fig. S3 B; and Table
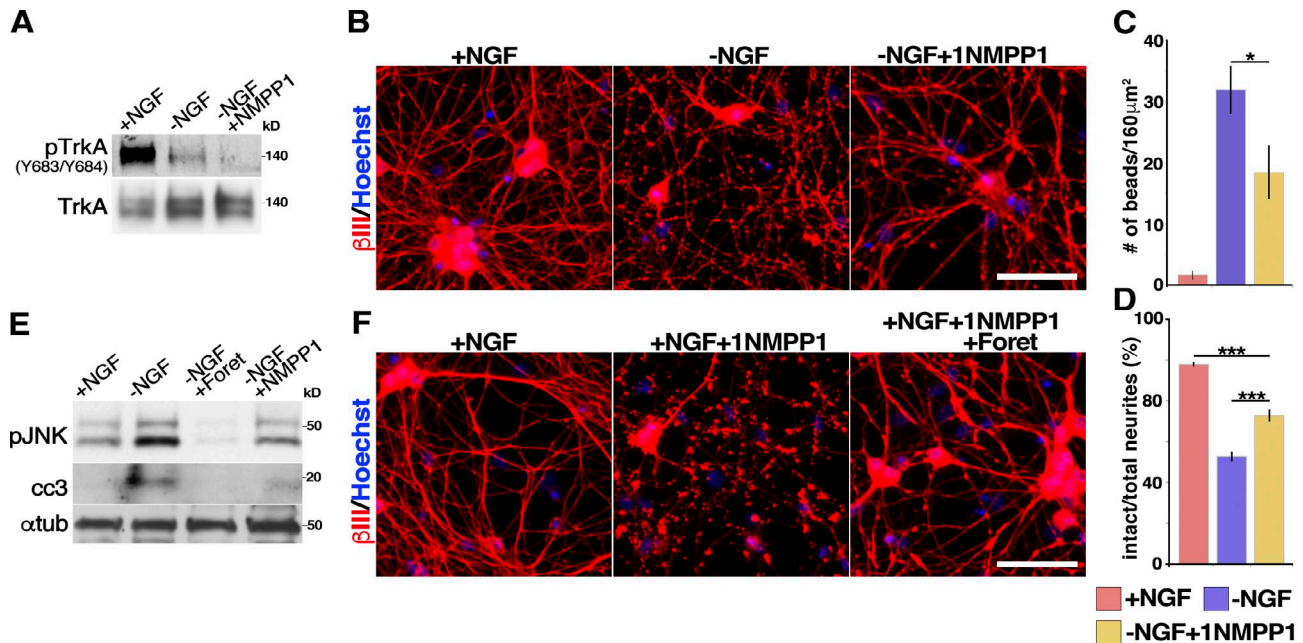
Figure 6. **TrkA inhibition partially rescues sympathetic neuron degeneration.** (A) WB analysis of TrkA^{F592A} sympathetic neurons withdrawn from NGF in the presence of 1 μM 1NMPP1 for 10 h, probed for Trk phosphorylated at Y683/Y684, and reprobed for total TrkA. (B) The specific TrkA^{F592A} inhibitor 1NMPP1 partially rescues NGF withdrawal-induced degeneration. TrkA^{F592A} sympathetic neurons cultured withdrawn from NGF in the presence or absence of 1 μM 1NMPP1 for 14 h and immunostained for βIII-tubulin and counterstained with Hoechst 33258. (C and D) Images as in B were quantified for the number of swellings or beads or for the ratio of intact neurites. (C) *, P < 0.05. (D) ***, P < 0.005; $n \geq 4$ independent experiments. (E) WB analysis of TrkA^{F592A} sympathetic neurons withdrawn from NGF in the presence of 500 nM foretinib (Foret) or 1 μM 1NMPP1 for 10 h, and probed for phosphorylated JNK (pJNK) and cleaved caspase-3 (cc3) and reprobed for total α-tubulin as a loading control. (F) Foretinib rescues axon degeneration that occurs at later time points in 1NMPP1. TrkA^{F592A} sympathetic neurons switched into NGF-containing medium with or without 1 μM 1NMPP1 or 500 nM foretinib for 24 h. Bars, 100 μm. Error bars represent mean ± SEM. All WB experiments were performed a minimum of three times, with representative blots shown.

S1). However, although these data indicate that there were similarities between the mechanisms of action of lestaurtinib and foretinib at these earlier time points, there were two notable differences. First, although lestaurtinib inhibited degeneration at early time points, by between 2 and 3 d after NGF withdrawal, murine sympathetic neurons had completely degenerated, whereas foretinib maintained axonal survival for at least 7 d (Fig. 1 E). Second, lestaurtinib but not foretinib caused the death of murine sympathetic neurons cultured in the presence of NGF within 2 to 3 d (unpublished data), indicating that only foretinib can rescue neuronal cell bodies.

These findings surprisingly suggest that residual TrkA kinase activity in NGF-deprived neurons may mediate a neuronal degeneration signal. To more definitively ask if this was the case, we turned to mice harboring a knock-in mutation in endogenous TrkA (F592A), rendering it susceptible to inhibition by 1NMPP1, a compound that inhibits no other known kinase in neurons (Chen et al., 2005). Sympathetic neurons from neonatal TrkA^{F592A} mice were cultured for 2 d, withdrawn from NGF in the presence of anti-NGF, and cultured with or without 1 μM 1NMPP1. Similar to the effects of foretinib and lestaurtinib, 1NMPP1 blocked the residual TrkA phosphorylation that was seen 10 h after NGF withdrawal (Fig. 6 A and Table S1). Because TrkA^{F592A} sympathetic neurons withdrawn from NGF begin to exhibit signs of advanced axonal degeneration 2–3 h earlier than those derived from *wt* mice, we analyzed these neurons 14 h after NGF withdrawal. Immunostaining for βIII-tubulin revealed that after NGF withdrawal, inhibition of TrkA activity with 1NMPP1 significantly rescued axonal degeneration, although the extent of rescue was less robust then

with foretinib (Fig. 6, B–D). WB analyses 8–10 h after NGF withdrawal showed that 1NMPP1 also partially suppressed the phosphorylation of JNK and the appearance of cleaved caspase-3 (Fig. 6 E and Table S1). The suppression of these responses by 1NMPP1 was not as effective as seen with lestaurtinib, consistent with the reduced rescue of the degeneration of TrkA^{F592A} axons by 1NMPP1.

Together with the lestaurtinib experiments, these data suggest that the low levels of TrkA activation observed after NGF withdrawal are important for neuronal degeneration of cultured neurons. However, the observation that foretinib is more effective than lestaurtinib or 1NMPP1 indicates that foretinib must suppress other degeneration pathways. To test this idea directly, we cultured neonatal TrkA^{F592A} sympathetic neurons in NGF and after 2 d added 1NMPP1 with or without foretinib. When only 1NMPP1 was added to these cultures, sympathetic neurons completely died after 24 h, even in the presence of NGF, because of inhibition of TrkA-dependent survival signaling. In contrast, foretinib completely rescued these neurons lacking TrkA activity from death and degeneration (Fig. 6 F). Thus, although inhibition of basal TrkA activity in the absence of NGF is likely important for a portion of foretinib's prosurvival activity, foretinib must inhibit additional kinases to efficiently suppress neuronal death.

Foretinib suppresses chemotherapy-induced axonal degeneration

We next asked whether foretinib could inhibit axonal degeneration in pathological conditions. Because chemotherapeutic agents are a major clinically relevant cause of axonal damage,

we asked whether it delayed axonal degeneration caused by the chemotherapeutic drug vincristine that prevents microtubule polymerization (Jordan et al., 1985). Mass cultures of neonatal rat sympathetic neurons established in NGF for 6 d were treated with 40 nM vincristine with or without foretinib. 10 h of exposure to vincristine caused extensive axonal degradation, and foretinib rescued this so that almost threefold more axons were maintained at this time point (Fig. 7, A and B). In these neurons, foretinib, as in neurons withdrawn from NGF, suppressed the increases in proapoptotic *bimEL* mRNA (Fig. 7 C). We also examined the activity of MKK4, a rate-limiting MKK that activates JNK and that is important for Wallerian degeneration (Yang et al., 2015) in vincristine-treated neurons that degenerate by a Wallerian degeneration-like process (Wang et al., 2000). To do this, mouse sympathetic neurons were exposed to vincristine for 1 h and were lysed and immunoblotted with antibodies specific for activated, phosphorylated MKK4 or for its downstream substrate JNK. This analysis showed that phosphorylation and activation of both MKK4 and JNK were suppressed by foretinib treatment (Fig. 7 D and Table S1). Finally, we asked about cisplatin, a chemotherapeutic agent that acts by interfering with DNA repair (Wang and Lippard, 2005), establishing mouse sympathetic neurons for 2 d, and then adding 20 µM cisplatin for 24 h. Foretinib partially rescued axonal degeneration in cultures exposed to cisplatin (Fig. S5, A and B).

In axons severed from cell bodies, foretinib suppresses Wallerian degeneration–associated signaling pathways, maintains ATP levels, and protects mitochondria

Both axonal die-back and Wallerian degeneration, in which axons are severed from their cell bodies, are the major pathological events in nerve injury and neurodegenerative conditions (Gerdts et al., 2016). To assess whether foretinib affects Wallerian degeneration, we established compartmented cultures of rat sympathetic neurons for 6 d in NGF and then removed the cell bodies and proximal axons from the central compartments, maintaining NGF in the side compartments. Immunostaining for βIII-tubulin showed that under these conditions, the isolated distal axons rapidly degenerated, until by 16 h they were almost completely fragmented (Fig. 7, E and F). In contrast, when foretinib was added to the axonal compartment 10 min before severing the cell bodies, the distal axons were largely intact 16 h after injury (Fig. 7, E and F). However, this was a delay and not a rescue, because by ∼36 h, the foretinib-treated axons had degenerated (unpublished data). To further address the idea that foretinib inhibited the Wallerian degeneration pathway in axons, we examined isolated sympathetic axons. Neonatal mouse superior cervical ganglia were cultured as explants in NGF for 4–5 d, and the ganglia were removed, leaving only the injured axons, which degenerated by 10–12 h after axotomy (Fig. S5, C and D). In contrast, when foretinib was present in the culture medium after the axotomy, the axons were largely intact at this time point (Fig. S5 D), as we had observed in compartmented cultures. WB analysis 15 min after ganglia removal showed that foretinib inhibited the phosphorylation of MKK4 and JNK, two kinases mediating Wallerian degeneration, relative to control, injured axons (Fig. 7 G and Table S1). Coincident with this axonal sparing, WB analysis after ganglia removal showed that foretinib prevented the JNK-dependent rapid degradation of the microtubule binding protein SCG10 (Shin et al., 2012) and the cleavage of the calpain substrates αII-spectrin, axonal

neurofilament L, and α-internexin (Fig. 7, H and I; and Table S1). Finally, by measuring ATP levels 6 and 9 h after axotomy (Wang et al., 2005; Gerdts et al., 2015; Yang et al., 2015), we found that foretinib significantly inhibited ATP depletion in the isolated axons (Fig. 7 K).

These data suggest that foretinib delays the degeneration of injured axons in axotomized sympathetic neurons in culture at least in part by inhibiting JNK signaling, thus preventing energy depletion and cytoskeletal degradation. Because foretinib has been reported not to directly inhibit JNK (Dufies et al., 2011), we next asked whether foretinib can act by inhibiting other elements of the Wallerian degeneration signaling cascade that function downstream of JNK signaling (Walker et al., 2017). A key pathway that maintains axonal energy homeostasis and preserves the integrity of axons is the conversion of prodegenerative nicotinamide mononucleotide (NMN) to neuroprotective NAD$^+$ by NMNAT2. After axotomy, NAD$^+$ levels decrease and NMN levels increase because of a loss of axonal NMNAT2 and SARM1-mediated destruction of NAD$^+$ (Wang et al., 2005; Osterloh et al., 2012; Shen et al., 2013; Di Stefano et al., 2015; Gerdts et al., 2016; Sasaki et al., 2016). To ask if foretinib can suppress axon degeneration caused by increases in prodegenerative NMN (Di Stefano et al., 2015; Loreto et al., 2015), axons were treated with NMN 2 h after axotomy in the presence or absence of foretinib. As a control, axons were also treated with FK866 that interferes with the endogenous synthesis of NMN and delays Wallerian degeneration (Di Stefano et al., 2015). The incubation of the isolated axons with NMN significantly enhanced Wallerian degeneration at 9 h after axotomy (Fig. 7, L [top] and N), which was not rescued with treatment by FK866 (Fig. 7, L [middle] and N), as the exogenous NMN promoted degeneration in the absence of endogenous NMN. Foretinib, however, completely rescued NMN-induced degeneration at this time point (Fig. 7, L [middle] and N). Although neither FK866 nor foretinib alone protected axons from Wallerian degeneration at 48 h after axotomy, both drugs together afforded long-lasting protection of severed axons for up to 72 h (Fig. 7 M). Finally, we asked whether foretinib protected mitochondria in severed axons, as it did in NGF withdrawal–induced die-back axon degeneration. Nine hours after axotomy, there were few active mitochondria in lesioned axons compared with unlesioned axons as shown by tetramethylrhodamine, methyl ester, perchlorate (TMRM) labeling of active mitochondria. Foretinib treatment, however, resulted in the protection of active mitochondria coincident with the delay in Wallerian degeneration (Fig. 7, O and P). To confirm these findings, we monitored the dissipation of mitochondrial membrane polarization by assessing the voltage-dependent proteolytic processing of the mitochondrial inner membrane factor Opa1 (Duvezin-Caubet et al., 2006; Ishihara et al., 2006; Summers et al., 2014), a hallmark of mitochondrial dysfunction, in axon-only lysates 8 h after axotomy by WB analysis with anti-Opa1. Foretinib treatment suppressed Opa1 proteolytic processing (Fig. 7 J and Table S1).

Foretinib delays Wallerian degeneration after sciatic nerve crush

To ask whether foretinib also rescued axonal degeneration in vivo, we focused upon Wallerian degeneration after crush injury to the sciatic nerve, which contains sympathetic, sensory and motor axons. We administered 100 mg/kg foretinib, a dose used in preclinical studies to test anticancer efficacy (Otte et al., 2015) by oral gavage four times over 4 d to adult mice, crushed
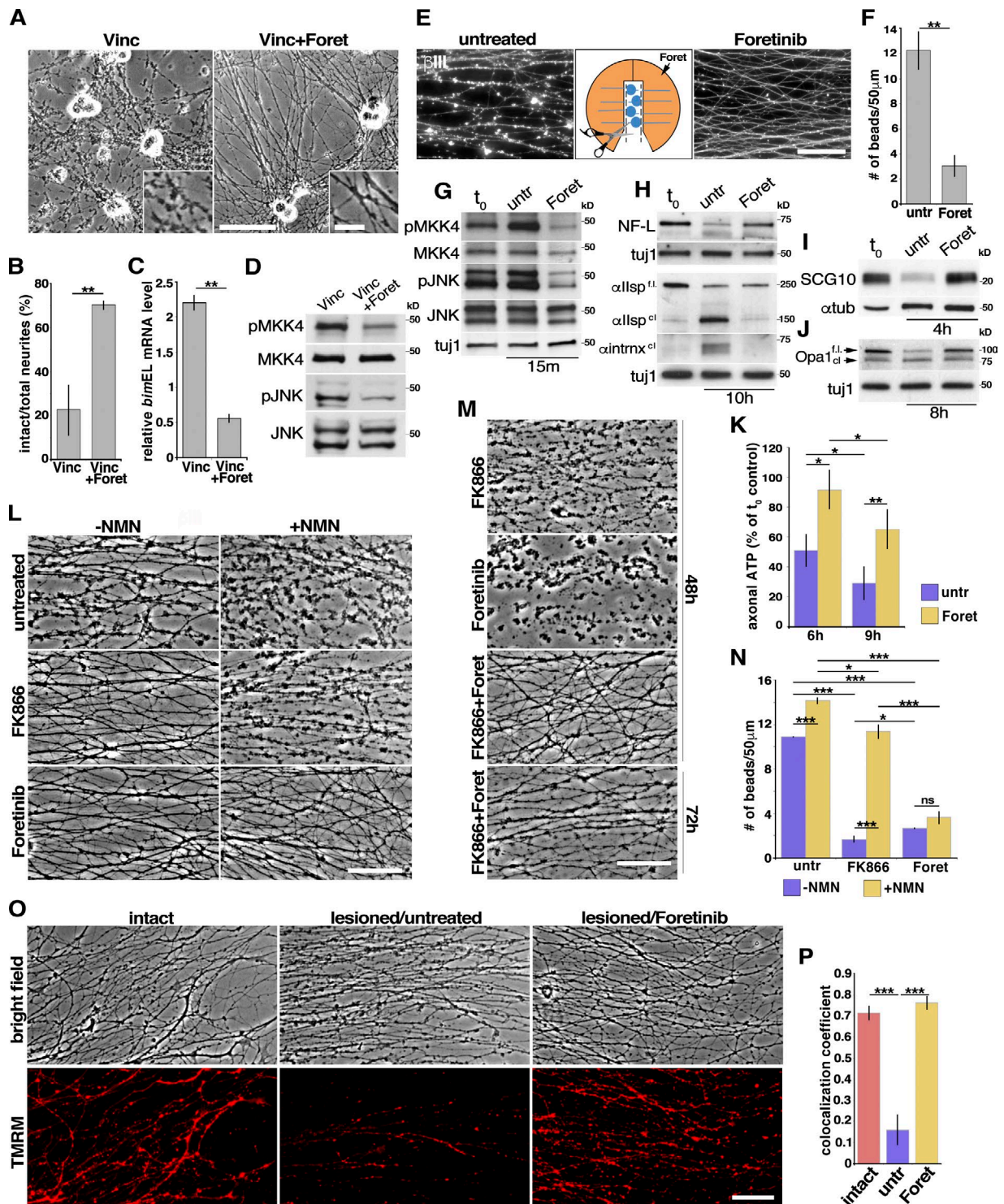
Figure 7. **Foretinib delays local axon degeneration caused by chemotherapeutic agents or axotomy and pro-Wallerian degeneration signaling.** (A) Bright-field micrographs of rat sympathetic neurons exposed to 40 nM of the chemotherapeutic agent vincristine (Vinc) with or without 500 nM foretinib (Foret) for 10 h. The insets show higher magnification views. (B) Ratio of intact neurites as in A. **, P < 0.01; $n \geq 3$ independent experiments. (C) Quantitative RT-PCR detected changes in *bimEL* mRNA levels as in A after 6 h; $n = 3$ independent experiments. **, P < 0.01. (D) WB of mouse sympathetic neurons treated with vincristine with or without foretinib for 1 h and probed for phosphorylated (p) and total MKK4 or phosphorylated and total JNK. (E) Foretinib delays Wallerian degeneration after axotomy. Compartmented cultures of rat sympathetic neurons where cell bodies and proximal axons were removed 15 min after the addition of 500 nM foretinib to one side compartment and immunostained for βIII-tubulin (white) 16 h after axotomy. Images show axons in the two side compartments of the same culture. (F) Quantification of the number of beads per 50 µm of neurites in the side compartments of cultures as in E. **, P < 0.01; $n \geq 3$ independent experiments. (G–J) WB analysis of isolated axons lysed 15 min (G), 10 h (H), 4 h (I), or 8 h (J) after cell body removal and probed with the indicated antibodies. (H) Neurofilament L (NF-L), αII-spectrin (αIIspec), anti-α-internexin (αintrnx); t_0 represents axons lysed immediately after isolation. (K) Axonal ATP levels measured 6 and 9 h after ganglia removal in the absence (control) or presence of foretinib, presented as the percentage of ATP in axons processed immediately after isolation (t_0 control). *, P < 0.05; **, P < 0.01; $n = 4$. (L and N) Foretinib suppresses axon degeneration caused by increases in prodegenerative NMN. Isolated mouse sympathetic neuron axons were cultured in foretinib or the endogenous NMN synthesis

the sciatic nerve 2 h after the fourth foretinib administration, and analyzed longitudinal sections of the nerve distal to the injury site at 48 h after crush by immunostaining for βIII-tubulin to distinguish axons. We also costained these sections for sodium channels to identify channel clusters at intact nodes of Ranvier (NORs), or for the paranodal protein Caspr to mark paranodal junctions between myelinating Schwann cells and axons (Feinberg et al., 2010; Fig. 8, A–C). In the injured distal nerve of vehicle-treated animals, there were fewer βIII-tubulin–positive axons than there were in uninjured nerves, and there were also many profiles characteristic of degenerating axons (Fig. 8, A, B, and D). In contrast, in mice treated with foretinib, there were significantly more apparently normal axon profiles although these were fewer than in uninjured nerves (Fig. 8, A, B, and D).

The double-labeling for sodium channels and Caspr also supported the idea that foretinib delayed Wallerian degeneration. In the distal injured nerves of vehicle-treated mice, there were only occasional sodium channel–positive NORs or Caspr-positive paranodal junctions, whereas in the foretinib-treated injured nerve, there were apparently many of both structures (Fig. 8, A–C). Quantification confirmed that there were two-to threefold more NORs and paranodal junctions in injured nerves from foretinib-treated mice than from vehicle-treated mice, although fewer than in the intact nerves (Fig. 8, E and F). Thus, foretinib delays Wallerian degeneration in vivo, as it does in culture.

Discussion

Here, we used a chemical biology approach to identify compounds that can potentially be used clinically to suppress axon degeneration and to identify novel targets mediating degeneration. Foretinib was the most potent drug found by screening a kinase inhibitor library that suppressed the NGF-induced degeneration of sympathetic neurons. Foretinib, as a Met/VEGFR inhibitor, has been assessed in several phase II clinical trials, including for papillary renal cell (Choueiri et al., 2013) and metastatic gastric cancer (Shah et al., 2013). The most common toxicities were like those seen in patients treated with other VEGFR inhibitors, including manageable hypertension, diarrhea, and fatigue (Choueiri et al., 2013). Foretinib is therefore a clinical candidate for the treatment of the many neurological and nerve injury-induced conditions in which axon degeneration is thought to be a crucial underlying pathological mechanism.

Foretinib was much more effective as an inhibitor of die-back or developmental cell body and axon degeneration than of Wallerian degeneration. The effect of foretinib was considerable, rescuing nearly 100% of sympathetic neurons and 60% of SOD mutant–overexpressing motor neurons deprived of trophic factors for 7 and 12 d, respectively. Foretinib acted locally, completely suppressing NGF withdrawal–induced axon degeneration (at the 48-h time point) when added to compartmented cultures in the axon-only chamber. This occurred even when

the cell bodies were dying. Intriguingly, in compartmented cultures deprived of NGF, foretinib added to the cell body compartment rescued untreated axons in the side compartment, indicating that foretinib can also suppress an axon degeneration signal emanating from the cell body that is transmitted anterogradely to the axon compartment. Our data indicate that this suppression may be mediated by inhibition of the expression of Puma, an axonal death protein functioning only in the cell body (Simon et al., 2016).

To understand how this agent suppresses or delays multiple types of degeneration in different paradigms, we initiated mechanistic studies to identify the targets of foretinib's activity. Regarding die-back degeneration, we and others have previously described the major degenerative pathway in these neurons involving MKK kinases that activate JNK and its transcriptional target c-jun (Kaplan and Miller, 2000; Culmsee and Mattson, 2005), the apoptotic p53 family member TAp63 (Jacobs et al., 2005; Yao et al., 2010), and the Bax activators BimEL and Hrk (Putcha et al., 2001; Towers et al., 2009), which in turn compromise mitochondria, culminating in cytochrome c release and activation of caspase-3 and caspase-6 and calpains (Slee et al., 1999). Foretinib inhibited the expression, appearance, or activity of these proteins, all of which are necessary for neuronal death or axon degeneration. Of particular importance is the inhibition of BimEL and Hrk expression, known to be rate limiting for sympathetic neuron cell body apoptosis (Imaizumi et al., 1997; Inohara et al., 1997; Kaplan and Miller, 2000; Putcha et al., 2001; Chang et al., 2002; Towers et al., 2009), and of Puma, which in sensory neurons initiates an anterograde prodegenerative signal (Simon et al., 2016). BimEL, Puma, and Hrk function in part by suppressing the activity of antiapoptotic BH3 family members known to be important in preventing peripheral neuron cell body and axon degeneration, including Bcl-2, Bcl-xL, and Bcl-w (Kaplan and Miller, 2000; Simon et al., 2016). Our data showing that foretinib potently suppresses expression of *bimEL*, *puma*, and *hrk* mRNAs, and that it does not rescue neurons in which the antiapoptotic BH3 family members are inhibited, suggest that foretinib acts by preserving the prosurvival activities of Bcl-2, Bcl-xL, and Bcl-w. Our findings also imply that foretinib ultimately functions by protecting mitochondria, because in the absence of NGF, it maintained mitochondrial membrane potential, suppressed cytochrome c release from mitochondria, and inhibited the ultimate activation of caspase-3, the initiator caspase for apoptosis and axon degeneration (Slee et al., 1999; Simon et al., 2012).

Regarding Wallerian degeneration, foretinib affected the degeneration pathway at multiple steps, suppressing MKK4/JNK activity, preserving ATP levels, maintaining antidegenerative SCG10 levels (Shin et al., 2012), and inhibiting calpain-induced cleavage of cytoskeletal proteins. We suggest that foretinib may transiently preserve NAD$^+$ levels, altering the balance of NMN versus NAD$^+$ in degenerating axons, thereby enabling the generation of ATP from oxidative phosphorylation or glycolysis. This could occur by foretinib-mediated suppression
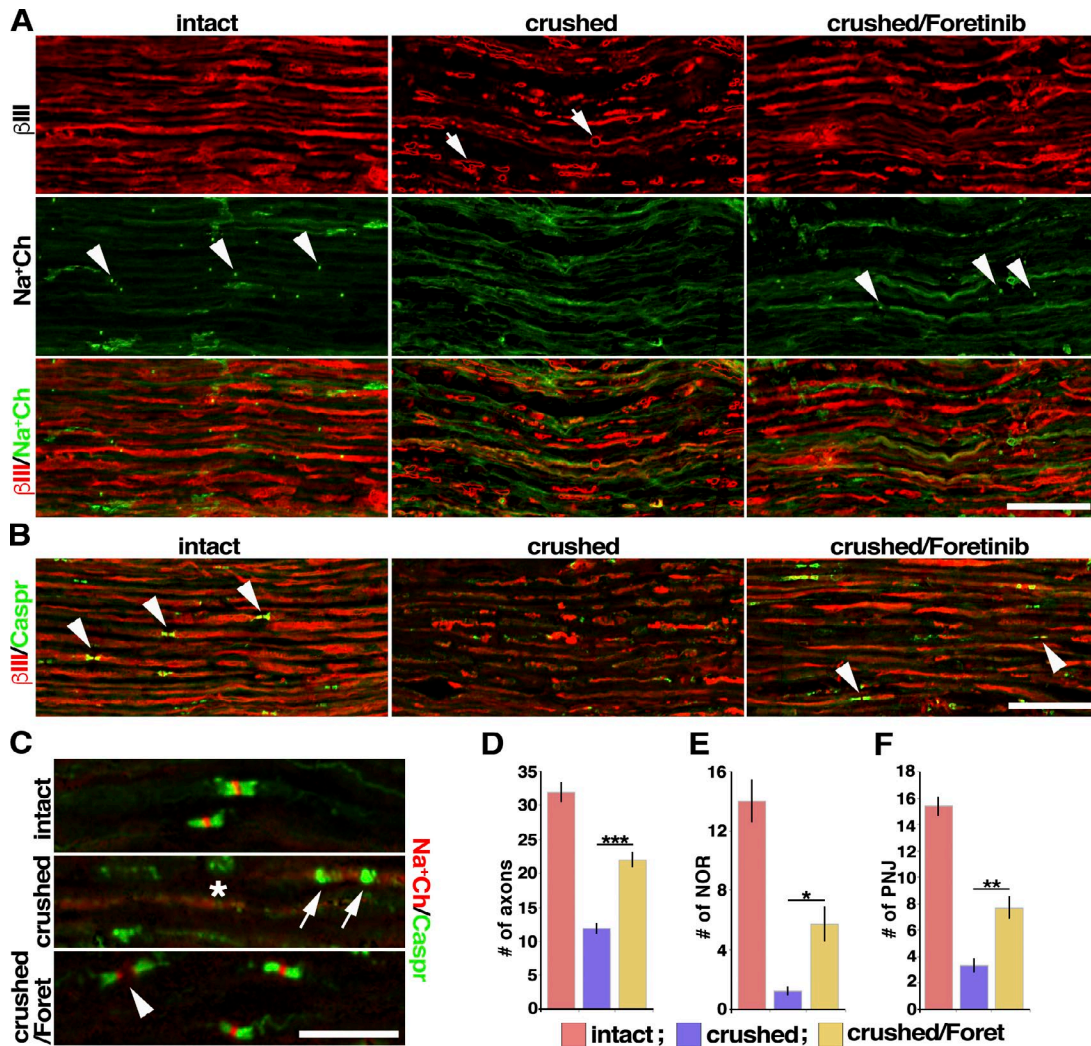
Figure 8. **Foretinib delays Wallerian degeneration after sciatic nerve injury.** 100 mg/kg foretinib (Foret) was administered to mice over 4 d, the sciatic nerve was unilaterally crushed 2 h after the final foretinib treatment, and 48 h later longitudinal sections of the distal nerve were analyzed by double-labeling for βIII-tubulin and total sodium channels (Na+Ch), Caspr to identify NORs, or paranodal junctions (PNJs). Extended-focus low-magnification (A and B) or high-magnification (C) confocal images of distal nerve sections from uninjured (intact), foretinib-treated injured (crushed/Foret), or DMSO-treated injured (crushed) mice, double-labeled for βIII-tubulin (red) and total sodium channels (green in A and red in C) or Caspr (green in B and C). Arrows denote abnormal axon shapes (A) or abnormal Caspr-positive PNJs (C), and arrowheads indicate apparently normal sodium channel-positive NORs (A), Caspr-positive PNJs (B) and dissociated NORs (C). Asterisk denotes diffused traces of Caspr staining. (D) Quantification of βIII-tubulin–positive axons, by counting positive profiles on randomly distributed lines of 200 µm throughout distal nerve sections as in A and B. ***, P < 0.005; n = 6 animals per group. Quantitation of the relative number of NORs (E) and PNJs (F) in randomly selected fields of 200 × 100 µm throughout the distal segments of nerves. *, P < 0.05; **, P < 0.01; n = 6 animals per group. Bars: (A and B) 50 µm; (C) 20 µm. Error bars represent mean ± SEM.

of SARM1 activity (which depletes NAD⁺) or by preventing the degradation of NMNAT2 (which preserves NAD⁺). Because mitochondrial energy metabolism and function are severely compromised in both Wallerian and die-back–induced degeneration (Yang et al., 2015; Persson et al., 2016), we therefore suggest that the efficacy of foretinib is due in large part to its ability to preserve mitochondrial function, and ATP levels in general.

What then is the direct target of foretinib in NGF-deprived axons? Our data indicate that it likely functions by inhibiting several direct targets, one of which is TrkA. Foretinib has been reported to inhibit TrkA activity at a similar half maximal inhibitory concentration as Met and VEGFR (Shi et al., 2009). In neurons withdrawn from NGF and treated with anti-NGF, we observed a low level of phosphorylation of TrkA by both phosphoproteomics and WB analysis with antibodies to the TrkA transphosphorylation sites. Inhibition of this low level of

TrkA activity with either foretinib or the Trk inhibitor lestaurtinib effectively rescued axons from degeneration. To confirm these findings, we used neurons that harbor a TrkA knock-in mutation that renders them susceptible to inhibition by 1NMPP1, which has no other known target (Chen et al., 2005). 1NMPP1 also partially rescued neurons from NGF-withdrawal induced degeneration, although it was less efficacious than foretinib.

Unliganded TrkA has been reported to induce the death of sympathetic neurons in culture and in vivo (Nikoletopoulou et al., 2010), although TrkA in that case was kinase inactive. Unliganded kinase-active TrkA induces the death of neural tumor cells and some aspects of survival in cultures of hippocampal neurons that aberrantly express TrkA (Harel et al., 2009; Matrone et al., 2009). In the sympathetic and hippocampal neuron studies, the effects of pro-death TrkA were mediated by p75NGFR (Matrone et al., 2009; Nikoletopoulou et al., 2010). We

report here, however, that in contrast to the long-term protective effects of foretinib, inhibition of TrkA activity in neurons with lestaurtinib or 1NMPP1 delays but does not inhibit degeneration. We suggest that unliganded active TrkA activates pro-death pathways, including those mediated by JNK and BimEL, and that NGF addition and hyperactivation of TrkA results in a switch whereby TrkA is coupled only to prosurvival signaling pathways. Kinase-active TrkA can induce the apoptosis of neural tumor cells by engaging CCM2 (Harel et al., 2009) or stimulating the activity of p53 (Lavoie et al., 2005). Although we have not observed changes in the activity of the CCM2 target and neuronal survival protein Erk5 with foretinib treatment (not depicted), we have observed a suppression of the transcription of the neuronal death protein and p53 family member TAp63 by foretinib (Fig. 4 B).

Inhibition of TrkA is only one of the mechanisms used by foretinib to prevent degeneration. First, foretinib potently rescued the trophic factor withdrawal-induced death of motor neurons that require glial cell-derived neurotrophic factor and brain-derived neurotrophic factor and not NGF for survival (Makhortova et al., 2011; Yang et al., 2013b). Second, in TrkA^{F592A} sympathetic neurons, inhibition of TrkA with 1NMPP1 only partially rescued the degeneration of neurons after NGF withdrawal, whereas foretinib completely rescued these neurons. Third, foretinib delayed Wallerian degeneration, which does not involve TrkA, in culture and in vivo. Fourth, Trk inhibitors, although prolonging axonal survival in NGF withdrawal conditions, ultimately caused neuronal death. What are the other foretinib targets? A clue comes from the Wallerian degeneration experiments. JNK and MKK4, an upstream activator of JNK, are important for both Wallerian and die-back degeneration, and our biochemical experiments showed that foretinib inhibited the activity of both kinases. These degeneration-inducing kinases speed the turnover of NMNAT2 that generates NAD$^+$ by converting NMN to NAD$^+$ (Gerdts et al., 2016; Walker et al., 2017), and foretinib, as a MKK/JNK inhibitor, could conceivable delay NMNAT2 degradation and NAD$^+$ loss after axotomy. Foretinib, however, may do so indirectly, because it is not a direct inhibitor of JNK in vitro (Dufies et al., 2011). Although it was stated in a review that foretinib bound to the JNK activator DLK, no supporting data were included or referenced (Ferraris et al., 2013). In addition, JNK inhibitors rescue sympathetic neurons from NGF withdrawal–induced degeneration for only 1–2 d and weakly suppress Wallerian degeneration. We suggest that the combination of unliganded TrkA and JNK pathway inhibition is responsible for a portion of foretinib's efficacious effects, at least in axons. There must, however, be yet another important degenerative pathway suppressed by Foretinib, because it rescues sympathetic neuron cell body apoptosis for as long as 7 d. The drug completely inhibited the transphosphorylation of NGF-induced TrkA in those cell bodies, indicating that foretinib acts by also inhibiting an as yet unidentified cell death pathway. Other possible candidates that we are currently assessing include PLCγ-1, which generates the second messenger inositol triphosphate, which facilitates calcium release from the endoplasmic reticulum, which in turn compromises mitochondria and induces axon degeneration (Villegas et al., 2014) and kinases that regulate the activity of DR6 and p75 neurotrophin receptor, both of which have been shown to initiate die-back and Wallerian degeneration (Nikolaev et al., 2009; Park et al., 2010; Gamage et al., 2017).

Materials and methods

Animals

All animal use was approved by The Hospital for Sick Children Animal Care Committee in accordance with Canadian Council of Animal Care policies. Mice homozygous for a TrkA^{F592A} gene (obtained from D. Ginty, Harvard University, Cambridge, MA) were maintained in a mixed CD1/C57BL6 background. CD1 mice and Sprague-Dawley rats (purchased from Charles River) were used for primary sympathetic and sensory neuron cultures. For sciatic nerve crush experiments, mice were anesthetized under isoflurane throughout entire procedure. At the end of every procedure, the wound was closed with staples, and mice were treated with analgesics (Anafen/Temgesic) after the surgery.

Primary sympathetic neuron cultures

For sympathetic neuron cultures, the SCGs of newborn Sprague-Dawley rats, CD1 mice, or TrkA^{F592A} mutant mice (Chen et al., 2005) were dissected as described (Park et al., 2010). For mass cultures, neurons were plated at a density of two rat ganglia per well or six mouse ganglia per well in 24-well dishes (for bright-field images and biochemical or molecular analyses), eight rat ganglia per well in 6-cm dishes (for microarray analysis), or one rat ganglion or three mouse ganglia per 13-mm glass slide (for immunohistochemistry [IHC] analysis). Rat and mouse neurons were plated on collagen and poly-D-lysine, respectively, as described (Feinberg et al., 2010; Park et al., 2010). For most experiments, mouse SCG neurons were grown for 2 d in growth media composed of UltraCULTURE media (Lonza), 2 mM L-glutamine (Lonza), and antibiotics (100 U/ml penicillin [Wisent] and 100 µg/ml streptomycin [Wisent]) and 30 ng/ml NGF (Almone Labs). Rat SCG neurons were grown in growth medium containing 87.5 ng/ml cytosine arabinoside (CA) and 3% FBS for 3 d and then switched to growth medium alone for an additional 3 d, as described (Park et al., 2010). Compartmented cultures were prepared and grown for 6 d as described (Park et al., 2010). For NGF withdrawal, neurons were washed twice with NGF-free culture medium and then cultured in UltraCULTURE medium without NGF and anti-NGF-β (1:1,000; Sigma-Aldrich). For the detection of BimEL and active Bax, mouse SCG neurons were grown as previously described (Putcha et al., 2001, 2003). In brief, the cultures were maintained for 5 d in Minimum Essential Medium (Life Technologies) containing 10% FBS (Life Technologies), L-glutamine and antibiotics, 20 µM uridine (Sigma-Aldrich), 20 µM 5-fluorodeoxyuridine (MP Biomedicals), 3.3 µg/ml aphidicolin (Tocris), and 50 ng/ml NGF. After 5 d, cultures were washed in NGF-free medium and subjected to experimental conditions in modified Eagle's medium supplemented with 10% FBS, L-glutamine and antibiotics, and neutralizing NGF antibody.

For Wallerian degeneration assay in compartments, axons were detached from their cell bodies by scratching the plates with a syringe needle at the sides of the cell body compartment and then washing the cell bodies out of the central compartment with medium from a 1-mm syringe with a 23-gauge PrecisionGlide needle. For Wallerian degeneration assays in 24-well plates, SCGs were dissected from neonatal CD1 mice and plated as explants on triple-coated (10 µg/ml poly-D-lysine, 10 µg/ml laminin, and 0.1 mg/ml collagen) wells and maintained in UltraCULTURE medium containing L-glutamine and antibiotics and 50 ng/ml NGF for 4 d after adhesion. Cultures were preincubated in 500 nM foretinib as applicable, and cell bodies were excised from neurites using a cut-tip 18.5-gauge needle. For WB analysis of axon-only lysates in Wallerian, SCGs from neonatal mice were cultured as ganglia for 5 d in vitro (DIV) on membranous Twiss filter inserts (1-µM pore; Torre and Steward, 1992; Zheng et al., 2001; Yang et al., 2013a) and

were axotomized and separated from the cell bodies by scraping the top of the membrane after treatment with drug or control conditions. The neurite-only portion on the bottom of the membrane was collected and lysed at indicated times after injury.

Primary sensory neuron cultures

Sensory neurons of E15 rat or E13 mouse DRGs were cultured as described (Feinberg et al., 2010). For immunostaining, neurons were plated at a density of 50×10^3 cells per 13-mm glass slide precoated with Matrigel (BD Biosciences), and poly-D-lysine (Sigma-Aldrich) as described (Feinberg et al., 2010). For phosphoproteomics, rat neurons were plated at a density of 10×10^6 cells per 10-cm dish coated with poly-D-lysine and laminin (Corning) as described (Feinberg et al., 2010). To eliminate non-neuronal cells, the day after plating, cultures were treated with 10 ng/ml CA for 2 d in growth medium composed of basal medium Eagle, ITS supplement, 0.2% BSA, 4 mg/ml D-glucose (all from Sigma-Aldrich), GlutaMAX (Gibco), 50 ng/ml NGF (Almone Labs), and antibiotics. Between CA treatments, the cultures were grown in NB medium, containing Neurobasal Medium (Gibco), GlutaMAX, 50 ng/ml NGF, B27 supplement (Gibco), and antibiotics for 2 days. After the second CA treatment, cultures were grown in NB medium for 1 additional day. For NGF-withdrawal experiments, neurons were washed twice with factor-free culture medium and then cultured in NB medium without NGF and including anti-NGF-β (1:1,000; Sigma-Aldrich).

Motor neuron cultures

Mouse ES cells were cultured in vitro and differentiated into motor neurons and plated in 96-well plates or 12-well plates as described (Makhortova et al., 2011; Yang et al., 2013b). For survival assays, motor neurons were seeded at a density of 30×10^3 GFP-positive cells (96-well plate) per well or 200×10^3 GFP-positive cells (12-well plate) per well. Trophic factors were removed after 3 d, and foretinib or DMSO was added. After an additional 3 d (day 6), cells were scanned using a high-content microscope (PerkinElmer Operetta) at 10× magnification. The number of motor neurons surviving was measured by counting the GFP-positive cells. For the long-term assays, the numbers of motor neurons were counted at days 6, 9, 11, and 15. CA was added into culture medium from day 2 as an antimitotic agent. Motor neuron cultures were fed with fresh medium every other day.

Kinase inhibitors screen

Rat SCG neurons were seeded at 3,000 cells per well in 100 µl medium in 96-well plates that were coated with collagen, as described (Park et al., 2010). Neurons were grown 3 d in growth medium containing 3% FBS and 87.5 ng/ml CA (Sigma-Aldrich), then switched to growth medium alone for an additional 3 d, and then infected with a previously described (Singh et al., 2008; Park et al., 2010) replication-deficient adenovirus expressing EGFP, as described (Park et al., 2010). One day later, the medium was replaced with growth medium for one more day, NGF was withdrawn, and the screen of a kinase inhibitor library (obtained from D. Uehling and R. Al-awar, Ontario Institute for Cancer Research, Toronto, ON, Canada) was performed as previously described (Grinshtein et al., 2011), with slight modifications. In brief, a kinase inhibitor library consisting of 480 drugs active against at least 60 individual kinases as primary targets was compiled by the Medicinal Chemistry Platform at the Ontario Institute for Cancer Research. Screening was performed at the S.M.A.R.T. Facility of Mt. Sinai Hospital, Toronto. Compounds were dissolved in DMSO, realiquoted in daughter plates as 1-mM solutions, and added using a pin tool to achieve a final concentration of 1 µM. Drug effects were compared with cells cultured with or without NGF plus 0.1% DMSO alone,

whereas wells filled with media served as the background. Neuronal survival was estimated under light and fluorescent microscopes 2, 3, and 4 d after NGF withdrawal.

Sciatic nerve crush

100 mg/kg foretinib (DMSO/H₂O/PEG 25:25:50) or vehicle alone was administered daily for 4 d. On the day of the fourth drug delivery, about 2 h after the gavage administration, sciatic nerves were unilaterally exposed and crushed by pinching with forceps for 30 s. The nerve was dissected 2 d after crush, fixed for 40 min on ice with 4% PFA and 15% sucrose, cryoprotected overnight in 30% sucrose containing PBS solution at 4°C, and cryosectioned longitudinally.

Immunostaining and mitochondrial labeling

Before immunostaining, neuronal cultures were fixed in 4% PFA on ice for 30 min for anticleaved caspase-3 or 10 min for all other antibodies. Nerve sections were permeabilized with methanol at −20°C for 5 min. Samples were then washed in PBS three times for 10 min each, incubated in primary antibodies overnight at 4°C, washed in PBS three times for 15 min, incubated with secondary antibodies 40 min at RT, washed three times in PBS, and mounted with PermaFluor (Thermo Fisher Scientific). Both primary and secondary antibodies were diluted in blocking solution, composed of PBS containing 0.1% Triton X-100 and 5% donkey serum. For mitochondrial labeling, live neuronal cultures were incubated with 50 nM MitoTracker Green FM and MitoTracker Red CMXRos (Life Technologies) after 24 h or 125 nM TMRM (VWR) 9 h after axotomy, using the manufacturer's protocols. Stained neuronal cultures and sciatic nerves were visualized using a Zeiss Axio Imager 2 microscope equipped with ApoTome2 and a Hamamatsu Digital Camera ORCA-flash4.0. Bright-field analysis of the same cultures was performed on a Zeiss Axiovert 200M. For Wallerian assays, SCGs from neonatal mice were cultured as ganglia for 5 DIV, axotomized, and treated with 125 nM TMRM (VWR) 9 h after axotomy. Axons were incubated with the mitochondrion-selective probes for 25 min at 37°, washed, and subsequently live-imaged using the Zeiss Cell Observer.

Microarrays

Two biological replicates each of rat sympathetic neuron cultures were analyzed with GeneChip Rat Gene 2.0 ST Array. Raw probe intensity values were background corrected, normalized with quantile normalization, transformed into the $\log_2$ scale, and summarized into probe sets using the Robust Multichip Analysis algorithm at the gene level in the Affymetrix Expression Console program. The averaged gene expression from two independent replicates was used to compare among groups. Genes showing >1.2-fold change between the "NGF + foretinib" and "−NGF" groups and having a nearly similar expression level compared with the "+NGF" group were chosen for further analysis (1,056 genes). The hierarchical clustering and heat-map analysis were performed using R and the heatmap.2 function from the gplot package with the Euclidean distance and complete linkage method.

Phosphoproteomics

E15 rat DRG sensory neuron cultures were grown in 10-cm dishes for 6 d and exposed to the experimental conditions for 8 h (four dishes per condition). Immediately before lysis, the cultures were treated with 1 mM sodium orthovanadate for 10 min. The neurons were lysed in urea lysis buffer (8 M urea and 20 mM Hepes, pH 8.0) containing phosphatase inhibitors (1 mM Na₃VO₄, 1 mM NaF, 1 mM β-glycerol phosphate, and 1.25 mM sodium pyrophosphate). The lysates were sonicated and cleared by centrifugation (20,000 g for 15 min at 15°C), and protein levels were quantified using Bradford analysis. Next, 45 mM DTT was

added to each sample at one tenth of a final volume and incubated at 60°C for 20 min, followed by the addition of 110 mM iodoacetamide for 15 min at RT in the dark. After dilution of samples to a final concentration of 2 M urea with 20 mM Hepes, pH 8.0, proteins were digested with 1 mg/ml TPCK-trypsin overnight at RT. The resultant peptide solutions were further purified using solid-phase extraction with Sep-Pak C18 (Waters UK) according to the manufacturer's instructions and lyophilized. Finally, phosphopeptides were enriched using PTMScan Phospho-Tyrosine Mouse mAb (P-Tyr-100) kit (5636; CST) according to the instructions.

Samples were analyzed on a linear ion trap Orbitrap hybrid analyzer (LTQ Orbitrap; Thermo Fisher Scientific) outfitted with a nanospray source and EASY-nLC split-free nano-LC system (Thermo Fisher Scientific). Lyophilized peptide mixtures were dissolved in 0.1% formic acid and loaded onto a 75 μm × 2 cm PepMap 100 Easy-Spray precolumn filled with 3 μm C18 beads followed by an in-line 75 μm × 50 cm PepMax RSLC EASY-Spray column filled with 2 μm C18 beads (Thermo Fisher Scientific) at a pressure of 600 bar. Peptides were eluted over 60 min at a rate of 250 nl/min using a 0–35% acetonitrile gradient in 0.1% formic acid. Peptides were introduced by nanoelectrospray into an LTQ Orbitrap hybrid mass spectrometer (Thermo Fisher Scientific). The instrument method consisted of one MS full scan (400–1,500 m/z) in the Orbitrap mass analyzer, an automatic gain control target of 1e6 with a maximum ion injection of 120 ms, one microscan, and a resolution of 240,000. Ten data-dependent MS/MS scans were performed in the linear ion trap using the 10 most intense ions at 35% normalized collision energy. The MS and MS/MS scans were obtained in parallel fashion. In MS/MS mode, automatic gain control targets were 1e5 with a maximum ion injection time of 50 msec. A minimum ion intensity of 5,000 was required to trigger an MS/MS spectrum. Normalized collision energy was set at 35. The dynamic exclusion was applied using a maximum exclusion list of 500 with one repeat count with a repeat duration of 30 s and exclusion duration of 8 s.

For database searching, tandem mass spectra were extracted, charge state deconvoluted, and deisotoped using Xcalibur v.2.2. All MS/MS samples were analyzed using Sequest v.1.4.1.14 (Thermo Fisher Scientific) and X! Tandem (version CYCLONE [2010.12.01.1]; The GPM). Sequest was set up to search Uniprot_Rattus_Norvegicus_Reviewed+Unreviewed_Nov272015.fasta (36,751 entries) assuming the digestion enzyme trypsin. X! Tandem was set up to search the Uniprot_Rattus_Norvegicus_Reviewed+Unreviewed_Nov272015 database (37,282 entries), also assuming trypsin. Sequest and X! Tandem were searched with a fragment ion mass tolerance of 0.60 D and a parent ion tolerance of 10.0 ppm. Carbamidomethyl of cysteine was specified in Sequest and X! Tandem as a fixed modification. Deamidated of asparagine and glutamine, oxidation of methionine, and phospho of serine, threonine, and tyrosine were specified in Sequest as variable modifications. Glu->pyro-Glu of the N terminus, ammonia loss of the N terminus, gln->pyro-Glu of the N terminus, deamidated of asparagine and glutamine, oxidation of methionine, and phospho of serine, threonine, and tyrosine were specified in X! Tandem as variable modifications.

Scaffold (version Scaffold_4.4.6; Proteome Software) was used to validate MS/MS-based peptide and protein identifications. Peptide identifications were accepted if they could be established at >95.0% probability. Peptide probabilities from X! Tandem were assigned by the Peptide Prophet algorithm (Keller et al., 2002) with Scaffold delta-mass correction. Peptide probabilities from Sequest were assigned by the Scaffold Local false discovery rate algorithm. Again, protein identifications were accepted if they could be established at >95.0% probability and contained at least one identified peptide. Protein probabilities were assigned by the Protein Prophet algorithm (Nesvizhskii et al., 2003). Proteins that contained similar peptides and could not be differentiated on the basis of MS/MS analysis alone were grouped to satisfy the principles of parsimony. A spectral library was built on the basis of all runs from the data set using Skyline software v.3.5.0.9191 (MacCoss Lab, University of Washington). MS1 extracted ion currents (XICs) for indicated phosphopeptides were extracted using Skyline software. The relative area of each XIC was normalized to XICs from two peptides of GAPDH and TUBA1A.

Quantitative RT-PCR analyses

For experiments with Bim, and Hrk, Puma/BBC3, Trib3, and Ddit3/CHOP, 2-DIV SCG cultures were exposed to experimental conditions with foretinib and lestaurtinib for 9 h. For experiments with p63, Noxa, and GADD45γ, 2-DIV SCG cultures were withdrawn from NGF and exposed to foretinib for 12 h. Bim and Hrk analysis for chemotherapy-treated cultures was conducted after cultures were treated for 6 h with NGF, 40 nM vincristine, or 40 nM vincristine and 500 nM foretinib. For all figures, results were normalized to *actb* mRNA and expressed as the fold increase relative to neurons in NGF. RNA was isolated using the Omega Bio-Tek EZNA Total RNA Kit and the RNase-free DNase I set (Omega Bio-Tek) according to the manufacturer's instructions. cDNA was prepared (SensiFAST cDNA Synthesis Kit; Bioline) and the added to the Sso Advanced Universal SYBR Green Supermix (Bio-Rad) PCR mixture. Analysis was performed on a CFX96 Touch Real-Time PCR Detection System (Bio-Rad). Data analysis was performed using Bio-Rad CFX Manager 3.1. *Actb* was used as the reference gene and values presented were calculated by $\Delta\Delta C_q$. Verified primers for *actb*, *bcl2l11/bimEL*, *hrk*, *puma/BBC3*, *Trib3*, *Ddit3*, *gadd45γ*, and *pmaip1/noxa* were obtained from Bio-Rad. Primers for *tap63* were obtained from Invitrogen with the sequences forward 5′-CGGAAGGCAGATGAAGAC AG-3′ and reverse 5′-GGGATCTCCGTTTCTTGATGG-3′.

Biochemical analysis

For whole-cell analysis, mouse sympathetic neuron cultures were lysed in TBS, 10% glycerol, and 1% NP-40 with 0.01 μg/ml aprotinin, 0.01 μg/ml leupeptin, 0.1 mM sodium vanadate, and 1 mM PMSF for 20 min on ice and centrifuged for 10 min at 4°C at 13,200 rpm. Supernatants were boiled for 5 min in SDS-PAGE sample buffer. For Wallerian degeneration analysis, at least 12 ganglia were pooled per condition. Axon-only lysates were prepared 10–12 h after axotomy for assessment of all proteins except phosphorylated MKK4/JNK, SCG10, and Opa1, analyzed 15 min, 4 h, and 8 h after axotomy, respectively. Axons were lysed in 2× Laemmli sample buffer with DTT and centrifuged for 10 min at 4°C at 13,200 rpm. Supernatants were collected, boiled for 5 min, and electrophoresed on 4–20% precast polyacrylamide gels. For active Bax detection, the cultures were lysed after 18 h of NGF withdrawal in nondenaturing and nonreducing lysis buffer (40 mM Hepes, pH 7.4, 120 mM NaCl, 1% CHAPS detergent, 1 mM EDTA, 1 mM EGTA, and 10% glycerol, with protease and phosphatase inhibitors [MS-SAFE inhibitor cocktail; Sigma-Aldrich]). Lysates were electrophoresed in native conditions on 4–20% Tris-glycine precast polyacrylamide gels (Bio-Rad) in Tris-glycine running buffer.

Preparation of cytosolic and mitochondrial subcellular fractions was performed essentially as described (Yang et al., 1997; Darios et al., 2003). In brief, neurons were lysed on ice for at least 10 min in 250 mM sucrose, 20 mM Tris-HCl, pH 7.5, 10 mM KCl, 1.5 mM MgCl₂, 1 mM EGTA, 1 mM EDTA, 1 mM DTT, 0.01 μg/ml aprotinin, 0.01 μg/ml leupeptin, 0.1 mM sodium orthovanadate, and 1 mM PMSF. Lysates were homogenized using a 30-gauge needle. 30 μl whole-cell lysate was set aside from each condition. Homogenates were centrifuged twice at 700 *g* for 10 min at 4°C, the S1 supernatant was collected, and SDS-PAGE sample buffer was added to the P1 pellet (nuclear fraction). The S1 supernatant was centrifuged at 10,000 *g* for 30 min at 4°C. The

P2 pellet (mitochondrial fraction) and supernatant S2 (the cytosolic fraction) were boiled for 5 min in SDS-PAGE sample buffer. Samples were electrophoresed on 4–20% precast polyacrylamide gradient gels (Bio-Rad), transferred to 0.45-µm nitrocellulose membranes, and blocked in 5% BSA TBST for 1 h at RT. Membranes were incubated overnight at 4°C with primary antibodies diluted in 5% BSA TBST, washed, and then incubated with secondary HRP-conjugated antibodies for 1 h at RT and visualized using a chemiluminescent detection reagent (ECL; Amersham).

Drugs
All drugs were kept in −20°C dissolved in DMSO in stock concentrations and were thawed and diluted to their final work concentrations in relevant medium immediately before addition to cell cultures. Drugs were as follows: foretinib (50 mM stock and 500 nM experimental; Selleckchem), lestaurtinib (50 mM stock and 1 µM experimental; Tocris), JNK inhibitor VII, TAT-TI-JIP$_{153–163}$ (10 mM stock and 2 µM experimental; Calbiochem), 1NMPP1 (25 mM stock; Calbiochem), vincristine (100 µM stock and 40 nM experimental; Selleckchem), cisplatin (50 mM stock and 20 µM experimental; Selleckchem), ABT263 (1 mM stock and 10 µM experimental; Selleckchem), and Z-VAD-FMK (0.5 M stock and 100 µM experimental; Calbiochem).

NMN and FK866 experiments
SCG ganglia from neonatal mice were cultured for 5 DIV, axotomized, treated with the indicated conditions (500 nM foretinib, 100 nM FK866 [Sigma-Aldrich], and/or 2 mM NMN [Sigma-Aldrich]), incubated for the indicated times (9, 48, and 72 h), and subsequently live-imaged. FK866 was added immediately after the axotomy, and NMN was added 2 h after axotomy.

Axonal ATP measurements
SCG ganglia were cultured in filter chambers as previously described, and the neurite-only portion on the bottom of the membrane was collected at the indicated times after injury, processed using the PerkinElmer ATPlite Luminescence System per the manufacturer's instructions, and assayed using the SpectraMax L Reader. Eight to ten ganglia were used per condition per experiment.

Antibodies
The following primary antibodies were used for IHC and WBs: anti–βIII-tubulin (rabbit, IHC, 1:1,000; PRB-435P; Covance), anti–βIII-tubulin (mouse, IHC, 1:1,000; MMS-435P; Covance), anti-caspr, (rabbit, IHC, 1:1,000, provided by E. Peles, Weizmann Institute, Rehovot, Israel), anti–pan Na+ channels (mouse, IHC, 1:1,000; S8809; Sigma-Aldrich); anti-GAPDH (rabbit, WB, 1:1,000; 14C10; Cell Signaling Technology), anti-ERK (rabbit, WB, 1:10,000; K-23; Santa Cruz Biotechnology), anti–phospho-ERK (rabbit, WB, 1:1,000; 9101; Cell Signaling Technology), anti-TrkA (rabbit, WB, 1:500; 2505; Cell Signaling Technology), anti–phospho-TrkA Tyr674/675 (rabbit, WB, 1:500; 4621; Cell Signaling Technology), anti-JNK (rabbit, WB, 1:500; 9251; Cell Signaling Technology), anti-Thr183/Tyr185 phospho-JNK (rabbit, WB, 1:500; 4668; Cell Signaling Technology), anti–cytochrome c (mouse, ICC, 1:550; 612302; BioLegend); anti-MKK4 (rabbit, WB, 1:1,000; 9152; Cell Signaling Technology); anti-Ser257/Thr261 phospho-MKK4 (rabbit, WB, 1:1,000; 9156; Cell Signaling Technology), anti-Ser63 phospho-c-Jun (rabbit, WB, 1:100; 9164; Cell Signaling Technology), anti-Bax (rabbit, WB, 1:500; 2772; Cell Signaling Technology), anti-(active) BAX 6A7 (mouse, WB, 1:100; B8429; Sigma-Aldrich), anti–spectrin αII chain (nonerythroid; mouse, WB, 1:500; MAB1622; EMD Millipore), anti–α-tubulin (mouse, WB, 1:1,000; T5168; Sigma-Aldrich), anti–cleaved caspase-3 (rabbit, WB,

1:100; IHC, 1:100; AB3623; EMD Millipore), anti-Bim/Bod (rabbit, WB, 1:1,000; ADI-AAP-330-E; Enzo Life Sciences), anti–neurofilament L (rabbit, WB, 1:1,000; 2837; Cell Signaling), anti–α-internexin (rabbit, 1:1,000; AB5354; Chemicon), anti-SCG10 (rabbit, 1:1,000; 10586-1-AP; Proteintech Group), and anti-Opa1 (rabbit, 1:750; 67589; Cell Signaling Technology). The following secondary antibodies (Jackson ImmunoResearch Laboratories) were used: goat anti–rabbit-HRP (1:13,000), goat anti–mouse-HRP (1:10,000), donkey anti–mouse-cy3 or 488 or cy5 (1:1,000), donkey anti–rabbit cy3 or 488 or cy5 (1:1,000), and donkey anti–rat 488 or cy5 (1:500).

Quantification
To quantify cell survival, 16 randomly dispersed squares of unit area 125 × 125 µm of Hoechst 33258–stained images were counted to quantify normal versus condensed, apoptotic nuclei. To quantify axonal degeneration in compartmented cultures, beads or swellings were counted along segments of neurites of 50–100-µm unit length, with 12 such segments counted per image per condition for at least three images per condition for each experiment. To quantify intact neurites and beads or swellings in mass cultures of sympathetic and sensory neurons, 16 squares of 40 × 40 µm size were placed at random along each image, and the intact (no fragmentation seen in the neurite segment within that square) versus total neurites within that field were counted. Beads along neurites categorized as broken (having one or more visible microtubule break) were also quantified. To quantify cytochrome c, 400 βIII-tubulin–positive immunostained neurons per condition per experiment were evaluated for lost or diffuse cytochrome c staining and presented as a percentage, three separate experiments in total. To quantify colocalization of MitoTrackers or TMRM signals in axons, fluorescent signal colocalization analysis was performed by Volocity software on the entire image per condition per experiment, three separate experiments in total. To quantify the amount of Wallerian degeneration in the injured sciatic nerve, confocal images of the entire sciatic nerve longitudinal sections were taken and then processed using tiling and extended depth focus functions, respectively, by ZEN software (Zeiss). Intact βIII-tubulin–positive axons were counted per 12 × 200 µm randomly distributed lines positioned perpendicularly to axonal growth. Caspr-positive paranodal junctions and Na+ channel–positive NORs were counted in 9 × 26,000 µm² randomly distributed rectangles along the length of the distal sciatic nerve sections. All images were processed using Adobe Photoshop, ImageJ, or Volocity. For quantitative analysis of WBs, Gel-Quant (DNR Bio-Imaging Systems) was used, analyzing at least three separate experiments per protein.

Statistical analysis
In experiments in which two groups were compared, t-test analysis was used. In experiments in which multiple samples were compared, statistical significance was determined using a one-way ANOVA with Tukey's or Dunnet's multiple-comparison test.

Online supplemental material
Fig. S1 contains supporting data showing that foretinib protects sympathetic neurons from degeneration more effectively than a selective JNK inhibitor at the 48-h time point. Fig. S2 contains supporting data showing that foretinib inhibits transcriptional and signaling events that occur during neuronal death and axonal degeneration in response to trophic factor withdrawal. Fig. S3 contains supporting data showing that foretinib and the Trk inhibitor lestaurtinib protect mitochondria and prevent the activation of caspase-3 in NGF-withdrawn sympathetic neurons. Fig. S4 contains supporting data showing that foretinib inhibits the tyrosine phosphorylation of TrkA at the site responsible for PLCγ1 association and the tyrosine phosphorylation of PLCγ1 in sensory neurons

deprived of NGF. Fig. S5 contains supporting data showing that foretinib delays cisplatin- or axotomy-induced axonal degeneration. Table S1 is the quantitative analysis of WBs presented in the study. Table S2 is the list of 1,056 genes whose expression is up-regulated by NGF withdrawal of sympathetic neurons and suppressed by foretinib.

References

Adalbert, R., and M.P. Coleman. 2013. Review: Axon pathology in age-related neurodegenerative disorders. *Neuropathol. Appl. Neurobiol.* 39:90–108. http://dx.doi.org/10.1111/j.1365-2990.2012.01308.x

Barr, R.K., I. Boehm, P.V. Attwood, P.M. Watt, and M.A. Bogoyevitch. 2004. The critical features and the mechanism of inhibition of a kinase interaction motif-based peptide inhibitor of JNK. *J. Biol. Chem.* 279:36327–36338. http://dx.doi.org/10.1074/jbc.M402181200

Besirli, C.G., E.F. Wagner, and E.M. Johnson Jr. 2005. The limited role of NH2-terminal c-Jun phosphorylation in neuronal apoptosis: Identification of the nuclear pore complex as a potential target of the JNK pathway. *J. Cell Biol.* 170:401–411. http://dx.doi.org/10.1083/jcb.200501138

Campenot, R.B. 2009. NGF uptake and retrograde signaling mechanisms in sympathetic neurons in compartmented cultures. *Results Probl. Cell Differ.* 48:141–158. http://dx.doi.org/10.1007/400_2009_7

Chang, L.K., G.V. Putcha, M. Deshmukh, and E.M. Johnson Jr. 2002. Mitochondrial involvement in the point of no return in neuronal apoptosis. *Biochimie.* 84:223–231. http://dx.doi.org/10.1016/S0300-9084(02)01372-X

Chen, X., H. Ye, R. Kuruvilla, N. Ramanan, K.W. Scangos, C. Zhang, N.M. Johnson, P.M. England, K.M. Shokat, and D.D. Ginty. 2005. A chemical-genetic approach to studying neurotrophin signaling. *Neuron.* 46:13–21. http://dx.doi.org/10.1016/j.neuron.2005.03.009

Choueiri, T.K., U. Vaishampayan, J.E. Rosenberg, T.F. Logan, A.L. Harzstark, R.M. Bukowski, B.I. Rini, S. Srinivas, M.N. Stein, L.M. Adams, et al. 2013. Phase II and biomarker study of the dual MET/VEGFR2 inhibitor foretinib in patients with papillary renal cell carcinoma. *J. Clin. Oncol.* 31:181–186. http://dx.doi.org/10.1200/JCO.2012.43.3383

Culmsee, C., and M.P. Mattson. 2005. p53 in neuronal apoptosis. *Biochem. Biophys. Res. Commun.* 331:761–777. http://dx.doi.org/10.1016/j.bbrc.2005.03.149

Cunningham, M.E., R.M. Stephens, D.R. Kaplan, and L.A. Greene. 1997. Autophosphorylation of activation loop tyrosines regulates signaling by the TRK nerve growth factor receptor. *J. Biol. Chem.* 272:10957–10967. http://dx.doi.org/10.1074/jbc.272.16.10957

Darios, F., O. Corti, C.B. Lücking, C. Hampe, M.P. Muriel, N. Abbas, W.J. Gu, E.C. Hirsch, T. Rooney, M. Ruberg, and A. Brice. 2003. Parkin prevents mitochondrial swelling and cytochrome c release in mitochondria-dependent cell death. *Hum. Mol. Genet.* 12:517–526. http://dx.doi.org/10.1093/hmg/ddg044

Deshmukh, M., and E.M. Johnson Jr. 1998. Evidence of a novel event during neuronal death: Development of competence-to-die in response to cytoplasmic cytochrome c. *Neuron.* 21:695–705. http://dx.doi.org/10.1016/S0896-6273(00)80587-5

Di Giorgio, F.P., M.A. Carrasco, M.C. Siao, T. Maniatis, and K. Eggan. 2007. Non-cell autonomous effect of glia on motor neurons in an embryonic stem cell-based ALS model. *Nat. Neurosci.* 10:608–614. http://dx.doi.org/10.1038/nn1885

Di Stefano, M., I. Nascimento-Ferreira, G. Orsomando, V. Mori, J. Gilley, R. Brown, L. Janeckova, M.E. Vargas, L.A. Worrell, A. Loreto, et al. 2015. A rise in NAD precursor nicotinamide mononucleotide (NMN) after injury promotes axon degeneration. *Cell Death Differ.* 22:731–742. http://dx.doi.org/10.1038/cdd.2014.164

Dufies, M., A. Jacquel, G. Robert, T. Cluzeau, A. Puissant, N. Fenouille, L. Legros, S. Raynaud, J.P. Cassuto, F. Luciano, and P. Auberger. 2011. Mechanism of action of the multikinase inhibitor foretinib. *Cell Cycle.* 10:4138–4148. http://dx.doi.org/10.4161/cc.10.23.18323

Duvezin-Caubet, S., R. Jagasia, J. Wagener, S. Hofmann, A. Trifunovic, A. Hansson, A. Chomyn, M.F. Bauer, G. Attardi, N.G. Larsson, et al. 2006. Proteolytic processing of OPA1 links mitochondrial dysfunction to alterations in mitochondrial morphology. *J. Biol. Chem.* 281:37972–37979. http://dx.doi.org/10.1074/jbc.M606059200

Feinberg, K., Y. Eshed-Eisenbach, S. Frechter, V. Amor, D. Salomon, H. Sabanay, J.L. Dupree, M. Grumet, P.J. Brophy, P. Shrager, and E. Peles. 2010. A glial signal consisting of gliomedin and NrCAM clusters axonal Na+ channels during the formation of nodes of Ranvier. *Neuron.* 65:490–502. http://dx.doi.org/10.1016/j.neuron.2010.02.004

Ferraris, D., Z. Yang, and D. Welsbie. 2013. Dual leucine zipper kinase as a therapeutic target for neurodegenerative conditions. *Future Med. Chem.* 5:1923–1934. http://dx.doi.org/10.4155/fmc.13.150

Galehdar, Z., P. Swan, B. Fuerth, S.M. Callaghan, D.S. Park, and S.P. Cregan. 2010. Neuronal apoptosis induced by endoplasmic reticulum stress is regulated by ATF4-CHOP-mediated induction of the Bcl-2 homology 3-only member PUMA. *J. Neurosci.* 30:16938–16948. http://dx.doi.org/10.1523/JNEUROSCI.1598-10.2010

Gamage, K.K., I. Cheng, R.E. Park, M.S. Karim, K. Edamura, C. Hughes, A.J. Spano, A. Erisir, and C.D. Deppmann. 2017. Death receptor 6 promotes Wallerian degeneration in peripheral axons. *Curr. Biol.* 27:890–896. http://dx.doi.org/10.1016/j.cub.2017.01.062

Gerdts, J., E.J. Brace, Y. Sasaki, A. DiAntonio, and J. Milbrandt. 2015. SARM1 activation triggers axon degeneration locally via NAD$^+$ destruction. *Science.* 348:453–457. http://dx.doi.org/10.1126/science.1258366

Gerdts, J., D.W. Summers, J. Milbrandt, and A. DiAntonio. 2016. Axon self-destruction: New links among SARM1, MAPKs, and NAD+ metabolism. *Neuron.* 89:449–460. http://dx.doi.org/10.1016/j.neuron.2015.12.023

Ghosh, A.P., B.J. Klocke, M.E. Ballestas, and K.A. Roth. 2012. CHOP potentially co-operates with FOXO3a in neuronal cells to regulate PUMA and BIM expression in response to ER stress. *PLoS One.* 7:e39586. http://dx.doi.org/10.1371/journal.pone.0039586

Grinshtein, N., A. Datti, M. Fujitani, D. Uehling, M. Prakesch, M. Isaac, M.S. Irwin, J.L. Wrana, R. Al-Awar, and D.R. Kaplan. 2011. Small molecule kinase inhibitor screen identifies polo-like kinase 1 as a target for neuroblastoma tumor-initiating cells. *Cancer Res.* 71:1385–1395. http://dx.doi.org/10.1158/0008-5472.CAN-10-2484

Harel, L., B. Costa, M. Tcherpakov, M. Zapatka, A. Oberthuer, L.M. Hansford, M. Vojvodic, Z. Yang, Z.Y. Chen, F.S. Lee, et al. 2009. CCM2 mediates death signaling by the TrkA receptor tyrosine kinase. *Neuron.* 63:585–591. http://dx.doi.org/10.1016/j.neuron.2009.08.020

Huntwork-Rodriguez, S., B. Wang, T. Watkins, A.S. Ghosh, C.D. Pozniak, D. Bustos, K. Newton, D.S. Kirkpatrick, and J.W. Lewcock. 2013. JNK-mediated phosphorylation of DLK suppresses its ubiquitination to promote neuronal apoptosis. *J. Cell Biol.* 202:747–763. http://dx.doi.org/10.1083/jcb.201303066

Imaizumi, K., M. Tsuda, Y. Imai, A. Wanaka, T. Takagi, and M. Tohyama. 1997. Molecular cloning of a novel polypeptide, DP5, induced during programmed neuronal death. *J. Biol. Chem.* 272:18842–18848. http://dx.doi.org/10.1074/jbc.272.30.18842

Inohara, N., L. Ding, S. Chen, and G. Núñez. 1997. harakiri, a novel regulator of cell death, encodes a protein that activates apoptosis and interacts selectively with survival-promoting proteins Bcl-2 and Bcl-X(L). *EMBO J.* 16:1686–1694. http://dx.doi.org/10.1093/emboj/16.7.1686

Ishihara, N., Y. Fujita, T. Oka, and K. Mihara. 2006. Regulation of mitochondrial morphology through proteolytic cleavage of OPA1. *EMBO J.* 25:2966–2977. http://dx.doi.org/10.1038/sj.emboj.7601184

Jacobs, W.B., G. Govoni, D. Ho, J.K. Atwal, F. Barnabe-Heider, W.M. Keyes, A.A. Mills, F.D. Miller, and D.R. Kaplan. 2005. p63 is an essential proapoptotic protein during neural development. *Neuron.* 48:743–756. http://dx.doi.org/10.1016/j.neuron.2005.10.027

Jordan, M.A., R.H. Himes, and L. Wilson. 1985. Comparison of the effects of vinblastine, vincristine, vindesine, and vinepidine on microtubule dynamics and cell proliferation in vitro. *Cancer Res.* 45:2741–2747.

Kaplan, D.R., and F.D. Miller. 2000. Neurotrophin signal transduction in the nervous system. *Curr. Opin. Neurobiol.* 10:381–391. http://dx.doi.org/10.1016/S0959-4388(00)00092-1

Kaplan, D.R., B.L. Hempstead, D. Martin-Zanca, M.V. Chao, and L.F. Parada. 1991. The trk proto-oncogene product: A signal transducing receptor for nerve growth factor. *Science.* 252:554–558. http://dx.doi.org/10.1126/science.1850549

Keller, A., A.I. Nesvizhskii, E. Kolker, and R. Aebersold. 2002. Empirical statistical model to estimate the accuracy of peptide identifications made by MS/MS and database search. *Anal. Chem.* 74:5383–5392. http://dx.doi.org/10.1021/ac025747h

Kojima, S., K. Mayumi-Matsuda, H. Suzuki, and T. Sakata. 1999. Molecular cloning of rat GADD45γ, gene induction and its role during neuronal cell death. *FEBS Lett.* 446:313–317. http://dx.doi.org/10.1016/S0014-5793(99)00234-3

Koprivica, V., K.S. Cho, J.B. Park, G. Yiu, J. Atwal, B. Gore, J.A. Kim, E. Lin, M. Tessier-Lavigne, D.F. Chen, and Z. He. 2005. EGFR activation mediates inhibition of axon regeneration by myelin and chondroitin sulfate proteoglycans. *Science.* 310:106–110. http://dx.doi.org/10.1126/science.1115462

Kristiansen, M., and J. Ham. 2014. Programmed cell death during neuronal development: The sympathetic neuron model. *Cell Death Differ.* 21:1025–1035. http://dx.doi.org/10.1038/cdd.2014.47

Kristiansen, M., F. Menghi, R. Hughes, M. Hubank, and J. Ham. 2011. Global analysis of gene expression in NGF-deprived sympathetic neurons identifies molecular pathways associated with cell death. *BMC Genomics.* 12:551. http://dx.doi.org/10.1186/1471-2164-12-551

Lavoie, J.F., L. Lesauteur, J. Kohn, J. Wong, O. Furtoss, C.J. Thiele, F.D. Miller, and D.R. Kaplan. 2005. TrkA induces apoptosis of neuroblastoma cells and does so via a p53-dependent mechanism. *J. Biol. Chem.* 280:29199–29207. http://dx.doi.org/10.1074/jbc.M502364200

Loreto, A., M. Di Stefano, M. Gering, and L. Conforti. 2015. Wallerian degeneration is executed by an NMN-SARM1-dependent late Ca²⁺ influx but only modestly influenced by mitochondria. *Cell Reports.* 13:2539–2552. http://dx.doi.org/10.1016/j.celrep.2015.11.032

Makhortova, N.R., M. Hayhurst, A. Cerqueira, A.D. Sinor-Anderson, W.N. Zhao, P.W. Heiser, A.C. Arvanites, L.S. Davidow, Z.O. Waldon, J.A. Steen, et al. 2011. A screen for regulators of survival of motor neuron protein levels. *Nat. Chem. Biol.* 7:544–552. http://dx.doi.org/10.1038/nchembio.595

Matrone, C., R. Marolda, S. Ciafrè, M.T. Ciotti, D. Mercanti, and P. Calissano. 2009. Tyrosine kinase nerve growth factor receptor switches from prosurvival to proapoptotic activity via Aβ-mediated phosphorylation. *Proc. Natl. Acad. Sci. USA.* 106:11358–11363. http://dx.doi.org/10.1073/pnas.0904998106

Miknyoczki, S.J., C.A. Dionne, A.J. Klein-Szanto, and B.A. Ruggeri. 1999. The novel Trk receptor tyrosine kinase inhibitor CEP-701 (KT-5555) exhibits antitumor efficacy against human pancreatic carcinoma (Panc1) xenograft growth and in vivo invasiveness. *Ann. N. Y. Acad. Sci.* 880(1 CELL AND MOLE):252–262. http://dx.doi.org/10.1111/j.1749-6632.1999.tb09530.x

Naska, S., S.A. Yuzwa, A.P. Johnston, S. Paul, K.M. Smith, M. Paris, M.V. Sefton, A. Datti, F.D. Miller, and D.R. Kaplan. 2016. Identification of drugs that regulate dermal stem cells and enhance skin repair. *Stem Cell Rep.* 6:74–84. http://dx.doi.org/10.1016/j.stemcr.2015.12.002

Neame, S.J., L.L. Rubin, and K.L. Philpott. 1998. Blocking cytochrome c activity within intact neurons inhibits apoptosis. *J. Cell Biol.* 142:1583–1593. http://dx.doi.org/10.1083/jcb.142.6.1583

Nesvizhskii, A.I., A. Keller, E. Kolker, and R. Aebersold. 2003. A statistical model for identifying proteins by tandem mass spectrometry. *Anal. Chem.* 75:4646–4658. http://dx.doi.org/10.1021/ac0341261

Neukomm, L.J., and M.R. Freeman. 2014. Diverse cellular and molecular modes of axon degeneration. *Trends Cell Biol.* 24:515–523. http://dx.doi.org/10.1016/j.tcb.2014.04.003

Nikolaev, A., T. McLaughlin, D.D. O'Leary, and M. Tessier-Lavigne. 2009. APP binds DR6 to trigger axon pruning and neuron death via distinct caspases. *Nature.* 457:981–989. http://dx.doi.org/10.1038/nature07767

Nikoletopoulou, V., H. Lickert, J.M. Frade, C. Rencurel, P. Giallonardo, L. Zhang, M. Bibel, and Y.A. Barde. 2010. Neurotrophin receptors TrkA and TrkC cause neuronal death whereas TrkB does not. *Nature.* 467:59–63. http://dx.doi.org/10.1038/nature09336

Osterloh, J.M., J. Yang, T.M. Rooney, A.N. Fox, R. Adalbert, E.H. Powell, A.E. Sheehan, M.A. Avery, R. Hackett, M.A. Logan, et al. 2012. dSarm/Sarm1 is required for activation of an injury-induced axon death pathway. *Science.* 337:481–484. http://dx.doi.org/10.1126/science.1223899

Otte, A., F. Rauprich, J. von der Ohe, Y. Yang, F. Kommoss, F. Feuerhake, P. Hillemanns, and R. Hass. 2015. c-Met inhibitors attenuate tumor growth of small cell hypercalcemic ovarian carcinoma (SCCOHT) populations. *Oncotarget.* 6:31640–31658. http://dx.doi.org/10.18632/oncotarget.5151

Park, K.J., C.A. Grosso, I. Aubert, D.R. Kaplan, and F.D. Miller. 2010. p75NTR-dependent, myelin-mediated axonal degeneration regulates neural connectivity in the adult brain. *Nat. Neurosci.* 13:559–566. http://dx.doi.org/10.1038/nn.2513

Persson, A.K., J.G. Hoeijmakers, M. Estacion, J.A. Black, and S.G. Waxman. 2016. Sodium channels, mitochondria, and axonal degeneration in peripheral neuropathy. *Trends Mol. Med.* 22:377–390. http://dx.doi.org/10.1016/j.molmed.2016.03.008

Putcha, G.V., M. Deshmukh, and E.M. Johnson Jr. 1999. BAX translocation is a critical event in neuronal apoptosis: regulation by neuroprotectants, BCL-2, and caspases. *J. Neurosci.* 19:7476–7485.

Putcha, G.V., K.L. Moulder, J.P. Golden, P. Bouillet, J.A. Adams, A. Strasser, and E.M. Johnson. 2001. Induction of BIM, a proapoptotic BH3-only BCL-2 family member, is critical for neuronal apoptosis. *Neuron.* 29:615–628. http://dx.doi.org/10.1016/S0896-6273(01)00238-0

Putcha, G.V., S. Le, S. Frank, C.G. Besirli, K. Clark, B. Chu, S. Alix, R.J. Youle, A. LaMarche, A.C. Maroney, and E.M. Johnson Jr. 2003. JNK-mediated BIM phosphorylation potentiates BAX-dependent apoptosis. *Neuron.* 38:899–914. http://dx.doi.org/10.1016/S0896-6273(03)00355-6

Sasaki, Y., T. Nakagawa, X. Mao, A. DiAntonio, and J. Milbrandt. 2016. NMN AT1 inhibits axon degeneration via blockade of SARM1-mediated NAD(+) depletion. *eLife.* 5:5. http://dx.doi.org/10.7554/eLife.19749

Schlatterer, S.D., C.M. Acker, and P. Davies. 2011. c-Abl in neurodegenerative disease. *J. Mol. Neurosci.* 45:445–452. http://dx.doi.org/10.1007/s12031-011-9588-1

Shah, M.A., Z.A. Wainberg, D.V. Catenacci, H.S. Hochster, J. Ford, P. Kunz, F.C. Lee, H. Kallender, F. Cecchi, D.C. Rabe, et al. 2013. Phase II study evaluating 2 dosing schedules of oral foretinib (GSK1363089), cMET/VEGFR2 inhibitor, in patients with metastatic gastric cancer. *PLoS One.* 8:e54014. http://dx.doi.org/10.1371/journal.pone.0054014

Shen, H., K.L. Hyrc, and M.P. Goldberg. 2013. Maintaining energy homeostasis is an essential component of Wld(S)-mediated axon protection. *Neurobiol. Dis.* 59:69–79. http://dx.doi.org/10.1016/j.nbd.2013.07.007

Shi, H., L. Liu, J. Greger, and T. Gilmer. 2009. GSK1363089 inhibits MET and synergizes with HER targeted agents in MET amplified/over-expressed and HER1/HER2 amplified tumor cells. Cancer Res.69:Abstract 1746.

Shin, J.E., B.R. Miller, E. Babetto, Y. Cho, Y. Sasaki, S. Qayum, E.V. Russler, V. Cavalli, J. Milbrandt, and A. DiAntonio. 2012. SCG10 is a JNK target in the axonal degeneration pathway. *Proc. Natl. Acad. Sci. USA.* 109:E3696–E3705. http://dx.doi.org/10.1073/pnas.1216204109

Simon, D.J., R.M. Weimer, T. McLaughlin, D. Kallop, K. Stanger, J. Yang, D.D. O'Leary, R.N. Hannoush, and M. Tessier-Lavigne. 2012. A caspase cascade regulating developmental axon degeneration. *J. Neurosci.* 32:17540–17553. http://dx.doi.org/10.1523/JNEUROSCI.3012-12.2012

Simon, D.J., J. Pitts, N.T. Hertz, J. Yang, Y. Yamagishi, O. Olsen, M. Tešić Mark, H. Molina, and M. Tessier-Lavigne. 2016. Axon degeneration gated by retrograde activation of somatic pro-apoptotic signaling. *Cell.* 164:1031–1045. http://dx.doi.org/10.1016/j.cell.2016.01.032

Singh, K.K., K.J. Park, E.J. Hong, B.M. Kramer, M.E. Greenberg, D.R. Kaplan, and F.D. Miller. 2008. Developmental axon pruning mediated by BDNF-p75NTR-dependent axon degeneration. *Nat. Neurosci.* 11:649–658. http://dx.doi.org/10.1038/nn.2114

Slee, E.A., M.T. Harte, R.M. Kluck, B.B. Wolf, C.A. Casiano, D.D. Newmeyer, H.G. Wang, J.C. Reed, D.W. Nicholson, E.S. Alnemri, et al. 1999. Ordering the cytochrome c-initiated caspase cascade: hierarchical activation of caspases-2, -3, -6, -7, -8, and -10 in a caspase-9-dependent manner. *J. Cell Biol.* 144:281–292. http://dx.doi.org/10.1083/jcb.144.2.281

Summers, D.W., A. DiAntonio, and J. Milbrandt. 2014. Mitochondrial dysfunction induces Sarm1-dependent cell death in sensory neurons. *J. Neurosci.* 34:9338–9350. http://dx.doi.org/10.1523/JNEUROSCI.0877-14.2014

Torre, E.R., and O. Steward. 1992. Demonstration of local protein synthesis within dendrites using a new cell culture system that permits the isolation of living axons and dendrites from their cell bodies. *J. Neurosci.* 12:762–772.

Towers, E., J. Gilley, R. Randall, R. Hughes, M. Kristiansen, and J. Ham. 2009. The proapoptotic dp5 gene is a direct target of the MLK-JNK-c-Jun pathway in sympathetic neurons. *Nucleic Acids Res.* 37:3044–3060. http://dx.doi.org/10.1093/nar/gkp175

Tse, C., A.R. Shoemaker, J. Adickes, M.G. Anderson, J. Chen, S. Jin, E.F. Johnson, K.C. Marsh, M.J. Mitten, P. Nimmer, et al. 2008. ABT-263: A potent and orally bioavailable Bcl-2 family inhibitor. *Cancer Res.* 68:3421–3428. http://dx.doi.org/10.1158/0008-5472.CAN-07-5836

Upton, J.P., A.J. Valentijn, L. Zhang, and A.P. Gilmore. 2007. The N-terminal conformation of Bax regulates cell commitment to apoptosis. *Cell Death Differ.* 14:932–942.

Villegas, R., N.W. Martinez, J. Lillo, P. Pihan, D. Hernandez, J.L. Twiss, and F.A. Court. 2014. Calcium release from intra-axonal endoplasmic reticulum leads to axon degeneration through mitochondrial dysfunction. *J. Neurosci.* 34:7179–7189. http://dx.doi.org/10.1523/JNEUROSCI.4784-13.2014

Walker, L.J., D.W. Summers, Y. Sasaki, E.J. Brace, J. Milbrandt, and A. DiAntonio. 2017. MAPK signaling promotes axonal degeneration by speeding the turnover of the axonal maintenance factor NMNAT2. *eLife.* 6:e22540. http://dx.doi.org/10.7554/eLife.22540

Wang, D., and S.J. Lippard. 2005. Cellular processing of platinum anticancer drugs. *Nat. Rev. Drug Discov.* 4:307–320. http://dx.doi.org/10.1038/nrd1691

Wang, J., Q. Zhai, Y. Chen, E. Lin, W. Gu, M.W. McBurney, and Z. He. 2005. A local mechanism mediates NAD-dependent protection of axon degeneration. *J. Cell Biol.* 170:349–355. http://dx.doi.org/10.1083/jcb.200504028

Wang, M.S., Y. Wu, D.G. Culver, and J.D. Glass. 2000. Pathogenesis of axonal degeneration: Parallels between Wallerian degeneration and vincristine neuropathy. *J. Neuropathol. Exp. Neurol.* 59:599–606. http://dx.doi.org/10.1093/jnen/59.7.599

Whitfield, J., S.J. Neame, L. Paquet, O. Bernard, and J. Ham. 2001. Dominant-negative c-Jun promotes neuronal survival by reducing BIM expression and inhibiting mitochondrial cytochrome c release. *Neuron.* 29:629–643. http://dx.doi.org/10.1016/S0896-6273(01)00239-2

Yang, J., X. Liu, K. Bhalla, C.N. Kim, A.M. Ibrado, J. Cai, T.I. Peng, D.P. Jones, and X. Wang. 1997. Prevention of apoptosis by Bcl-2: Release of cytochrome c from mitochondria blocked. *Science.* 275:1129–1132. http://dx.doi.org/10.1126/science.275.5303.1129

Yang, J., R.M. Weimer, D. Kallop, O. Olsen, Z. Wu, N. Renier, K. Uryu, and M. Tessier-Lavigne. 2013a. Regulation of axon degeneration after injury and in development by the endogenous calpain inhibitor calpastatin. *Neuron.* 80:1175–1189. http://dx.doi.org/10.1016/j.neuron.2013.08.034

Yang, J., Z. Wu, N. Renier, D.J. Simon, K. Uryu, D.S. Park, P.A. Greer, C. Tournier, R.J. Davis, and M. Tessier-Lavigne. 2015. Pathological axonal death through a MAPK cascade that triggers a local energy deficit. *Cell.* 160:161–176. http://dx.doi.org/10.1016/j.cell.2014.11.053

Yang, Y.M., S.K. Gupta, K.J. Kim, B.E. Powers, A. Cerqueira, B.J. Wainger, H.D. Ngo, K.A. Rosowski, P.A. Schein, C.A. Ackeifi, et al. 2013b. A small molecule screen in stem-cell-derived motor neurons identifies a kinase inhibitor as a candidate therapeutic for ALS. *Cell Stem Cell.* 12:713–726. http://dx.doi.org/10.1016/j.stem.2013.04.003

Yao, J.Y., C.C. Pao, and J.K. Chen. 2010. Transcriptional activity of TAp63 promoter is regulated by c-jun. *J. Cell. Physiol.* 225:898–904. http://dx.doi.org/10.1002/jcp.22300

Zareen, N., S.C. Biswas, and L.A. Greene. 2013. A feed-forward loop involving Trib3, Akt and FoxO mediates death of NGF-deprived neurons. *Cell Death Differ.* 20:1719–1730. http://dx.doi.org/10.1038/cdd.2013.128

Zheng, J.Q., T.K. Kelly, B. Chang, S. Ryazantsev, A.K. Rajasekaran, K.C. Martin, and J.L. Twiss. 2001. A functional role for intra-axonal protein synthesis during axonal regeneration from adult sensory neurons. *J. Neurosci.* 21:9291–9303.